



HAL
open science

**A New Class of Rhodium(I) $\kappa 1$ -P and $\kappa 2$ -P, N
Complexes with Rigid PTN(R) Ligands (PTN =
7-Phospha-3-methyl-1,3,5-triazabicyclo[3.3.1]nonane)**

Andrew D Phillips, Sandra Bolaño, Sylvain S Bosquain, Jean-Claude Daran,
Raluca Malacea, Maurizio Peruzzini, Rinaldo Poli, Luca Gonsalvi

► **To cite this version:**

Andrew D Phillips, Sandra Bolaño, Sylvain S Bosquain, Jean-Claude Daran, Raluca Malacea, et al..
A New Class of Rhodium(I) $\kappa 1$ -P and $\kappa 2$ -P, N Complexes with Rigid PTN(R) Ligands (PTN
= 7-Phospha-3-methyl-1,3,5-triazabicyclo[3.3.1]nonane). *Organometallics*, 2006, 25 (9), pp.2189-2200.
10.1021/om051099r . hal-03196095

HAL Id: hal-03196095

<https://hal.science/hal-03196095>

Submitted on 12 Apr 2021

HAL is a multi-disciplinary open access archive for the deposit and dissemination of scientific research documents, whether they are published or not. The documents may come from teaching and research institutions in France or abroad, or from public or private research centers.

L'archive ouverte pluridisciplinaire **HAL**, est destinée au dépôt et à la diffusion de documents scientifiques de niveau recherche, publiés ou non, émanant des établissements d'enseignement et de recherche français ou étrangers, des laboratoires publics ou privés.

A new class of rhodium(I) κ^1 -*P* and κ^2 -*P,N* complexes
with rigid PTN(R) ligands (PTN = 7- phospho-3-
methyl-1,3,5-triazabicyclo[3.3.1]nonane)

*Andrew D. Phillips,^a Sandra Bolaño,^a Sylvain S. Bosquain,^a Jean-Claude Daran,^b Raluca Malacea,^b
Maurizio Peruzzini,^{a*} Rinaldo Poli,^{b*} and Luca Gonsalvi^{a*}*

^a Consiglio Nazionale delle Ricerche, Istituto di Chimica dei Composti Organometallici (ICCOM-CNR), Via Madonna del Piano 10, 50019 Sesto Fiorentino (Firenze), Italy. ^b Laboratoire de Chimie de Coordination (UPR CNRS 8241), 205 route de Narbonne, 31077 Toulouse Cedex 4, France.

l.gonsalvi@iccom.cnr.it, mperuzzini@iccom.cnr.it, poli@lcc-toulouse.fr

RECEIVED DATE (to be automatically inserted after your manuscript is accepted if required according to the journal that you are submitting your paper to)

ABSTRACT The open cage ligands PTN(R) (PTN = 7-R-phospha-3-methyl-1,3,5-triazabicyclo[3.3.1]nonane; R = Me, Ph), derived from cage cleavage of the water-soluble phosphine PTA (PTA = 1,3,5-triaza-7-phosphaadamantane), were used to synthesize neutral [RhCl(cod)(PTN(R))], (**10**) [RhI(CO){PTN(Me)}] (**12**) and cationic [Rh(cod){PTN(R)}][BAr^F₄] (**11**) rhodium (I) complexes which were comprehensively characterized both in solution and in the solid state (cod = 1,5-cyclooctadiene; BAr^F₄ = B[3,5-(CF₃)₂C₆H₃]₄). Two modes of coordination to the metal were identified, κ^1 -P (for **10**) and κ^2 -P,N (**11**, **12**). For κ^1 -P coordination, the free N donor site rests in close proximity to the Rh center thanks to the rigid PTN framework. The complexes were tested as catalysts for (biphasic) olefin hydroformylation and regioselective C=C bond reduction under transfer hydrogenation conditions, together with acetophenone hydrogenation. DFT calculations on simplified models helped to assess the electronic and bonding properties within the complexes and to determine the amount of cage strain that accompanies the structural modifications of the ligand when transformed from a κ^1 -P to κ^2 -P,N mode.

INTRODUCTION

During the last decade, ligand design for homogeneous catalysts has advanced from simple bidentate diphosphines and diamines to mixed donor atom moieties, such as phosphino-ethers, phosphino-thioethers and aminophosphines.¹ These catalytic systems have been applied to hydroformylation, hydrogenation and hydrosilylation reactions.^{2,3,4} Numerous configurations of phosphorus-nitrogen (P,N) ligands have been reported and can be generically divided into two categories, namely those based on structurally rigid *sp*² nitrogen centers, e.g. unsaturated pyridine⁵ and imine⁶ groups or *sp*³ nitrogen centers, which constitute saturated amine functionalities.^{7,8} For *sp*³ N-based ligands, rigidity is enforced either using a short (e.g. four atom) chain chelate,⁸ or by usually inserting a phenyl,⁹ pyridyl,¹⁰ ferrocenyl¹¹ or other functionalities containing π -bonding into the ligand backbone.¹²

Among aminophosphine ligands, the neutral water-soluble phosphine 1-phospha-3,5,7-triazaadamantane (PTA, **1**),¹³ was successfully used to prepare κ^1 -P-coordinated rhodium catalysts

capable of regioselective hydrogenation¹⁴ and hydroformylation¹⁵ of olefins in aqueous media. Long-term catalyst stability and low activity are two of the most problematic aspects for systems based on PTA,¹⁶ thus a shift from a monodentate to a bidentate hemilabile ligand system featuring similar stereoelectronic properties and water solubility could be of interest. On this basis we have considered the use of the bowl-shaped alkyl or aryl *P*-substituted 7-phospha-3-methyl-1,3,5-triazabicyclo[3.3.1]nonanes abbreviated as PTN(R) (**2**), synthesized originally by Schmidbaur et al.¹⁷

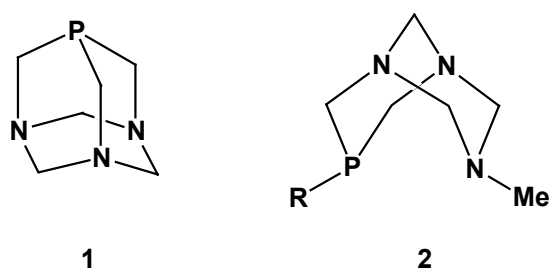
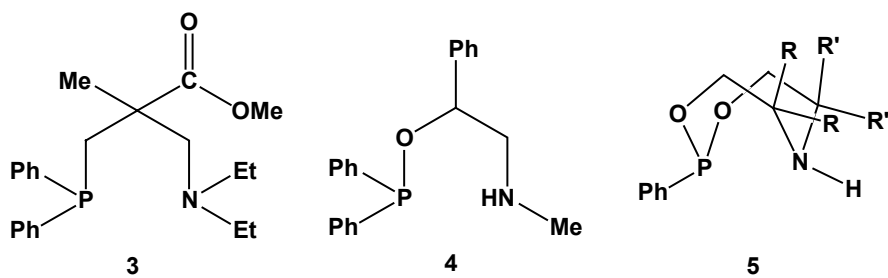


Chart 1

The bridgehead position of **2** anchors the ligand conformation, with the constrained curvature creating a preset bidentate capability. This structural feature is also advantageous in a non-chelating situation where the inflexible framework insures that the amine functionality remains always in close proximity of the transition metal center, a feature that has been suggested to facilitate the intramolecular base-assisted heterolytic cleavage of H₂.¹⁸ Other examples of chelated (κ^2 -*P,N*)-Rh complexes with aminophosphine (**3**),¹⁹ aminophosphinite (**4**),²⁰ and aminophosphinite (**5**)²¹ have been reported.



R = Me; R' = H, Me

Chart 2

The coordination chemistry of **2** has received so far scarce attention, including Au and Mo complexes (Chart 3). Depending on the nature of the ancillary substituent attached to Au, **2** adopts either a mono- or bi-dentate coordination mode,²² and examples of both were obtained as, [κ^1 -P-AuCl{PTN(R)}] (**6** R = Me, Ph), [κ^1 -P-AuCl{PTN(Me)}₂] (**7**), and [κ^2 -P,N-AuMe₂{PTN(Me)}][AuCl₄] (**8**), the latter exhibiting high water solubility. A second group of PTN(R) complexes containing molybdenum have also been reported by Schmidbaur and co-workers. Although no crystals suitable for X-ray diffraction studies were obtained, in all cases, the κ^2 -P,N coordination mode of **2** in [Mo(CO)₄{PTN(R)}] (**9**, R = Me, Ph) is inferred from the number and intensity of IR active CO stretching frequencies.²²

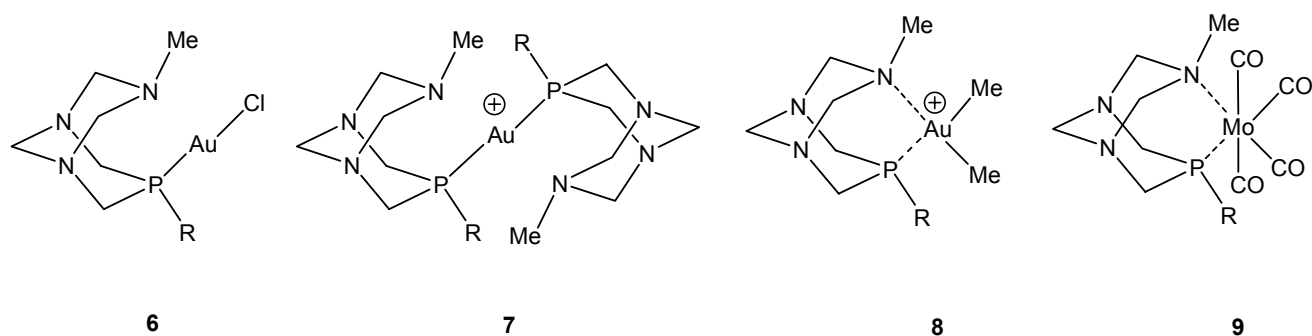


Chart 3

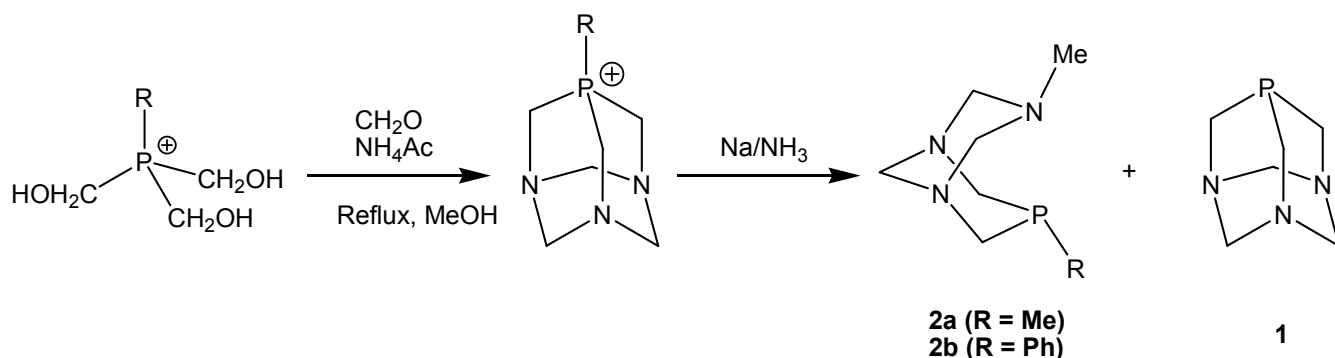
In this article we report the synthesis, spectroscopic and structural data together with a computational analysis of **2** ligated to rhodium (I) centers, in both a mono- and bidentate coordination mode. The complexes were tested as catalysts for olefin hydroformylation and transfer hydrogenation of benzylidene acetone and acetophenone in organic and biphasic organic/water solvent systems and the results are reported.

RESULTS AND DISCUSSION

Syntheses and characterizations of Rh(I) complexes with PTN(R) ligands

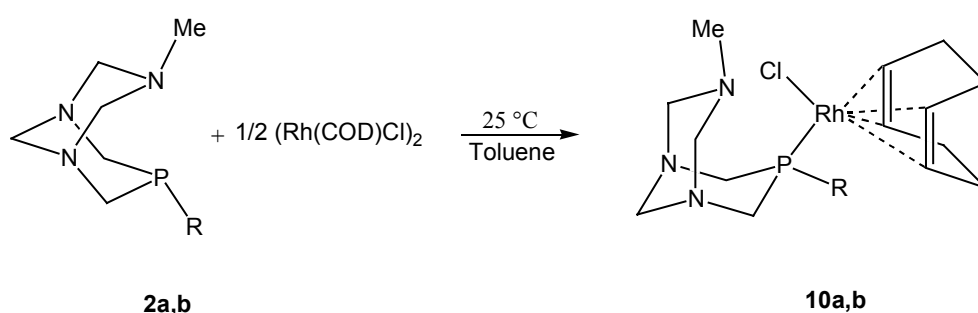
PTN(R) ligands were first described by Schmidbaur and co-workers, and were obtained by reductive cleavage of P-functionalized PTA salts (see Scheme 1).^{22,23} The choice of the substituent

on P was limited to R = Me, Ph as negligible yields are obtained for R = benzyl, cyclohexyl, *t*-butyl due to non-selective and inefficient cleavage.²²



Scheme 1

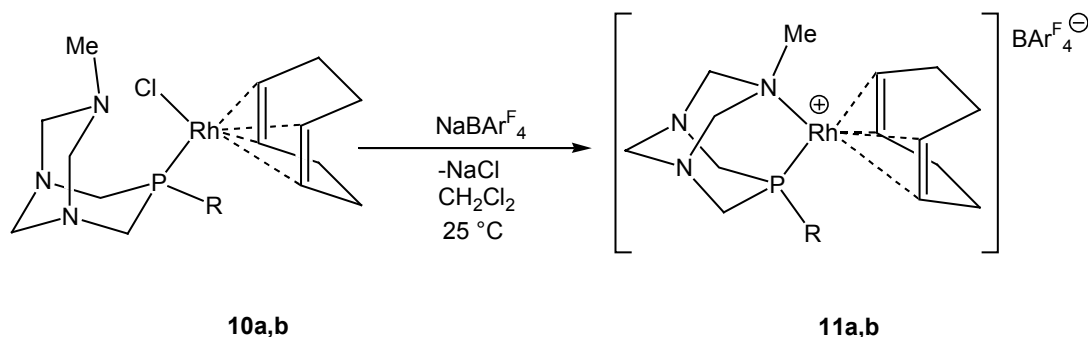
We synthesized and fully characterized two new classes of Rh(I) 1,5-cyclo-octadiene (COD) complexes, featuring **2** in a monodentate κ^1 -P or chelate κ^2 -P,N coordination mode. The preparation of the monodentate PTN(R) complexes from $[\text{Rh}(\text{cod})\text{Cl}]_2$ is straightforward (Scheme 2) and affords the products $[\text{RhCl}(\text{cod})\{\text{PTN}(\text{R})\}]$ (R = Me, **10a**; R = Ph, **10b**) as air and moisture stable yellow solids in high yields.



Scheme 2

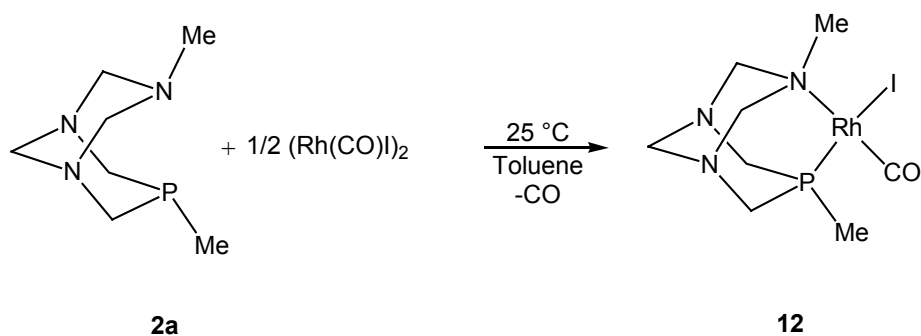
Complex **10a** is readily soluble in chlorinated solvents, toluene and benzene, and moderately soluble in water with $S(25\text{ }^\circ\text{C}) = 3.80\text{ mg ml}^{-1}$, at a value comparable to $[\text{RhCl}(\text{PTA})_3]$ ²⁴ and $[\text{Rh}(\text{acac})(\text{CO})(\text{PTA})]$.¹⁴ In contrast, the presence of the phenyl group on P atom significantly reduces the aqueous solubility for **10b**, $S(25\text{ }^\circ\text{C}) = 0.74\text{ mg ml}^{-1}$. Toluene solutions of **10** instantly produce black precipitates when heated beyond 100 °C, whereas of a sample of **10a** in D₂O heated to 80°C showed no change in the ³¹P{¹H} spectrum after 5h. Routine EI-MS characterization is reported in the Experimental Section.

Complexes **10** were reacted with one equivalent of $\text{NaB}(\text{C}_6\text{H}_3(\text{CF}_3)_2)_4$ (abbreviated as $\text{NaBAr}^{\text{F}_4}$)²⁵ in dichloromethane to afford κ^2 -*P,N* complexes $[\text{Rh}(\text{cod})\{\text{PTN}(\text{R})\}](\text{BAr}^{\text{F}_4})$ ($\text{R} = \text{Me}$, **11a**; $\text{R} = \text{Ph}$, **11b**, Scheme 3) which were isolated as air sensitive bright yellow compounds.



Scheme 3

The neutral, air and moisture sensitive rhodium complex k^2 -*P,N*- $[\text{RhI}(\text{CO})\{\text{PTN}(\text{Me})\}]$ (**12**) was obtained directly by reacting the dimer $\text{Rh}_2(\text{CO})_4\text{I}_2$ with two equivalents of **2a** in dichloromethane or toluene and stirring for 1 h at room temperature, as shown in Scheme 4. The water solubility of **12** [$S(25^\circ\text{C}) = 0.2 \text{ mg l}^{-1}$] is remarkably decreased from that of **11a** as for other neutral carbonyl complexes.



Scheme 4

The values for ${}^{31}\text{P}\{\text{H}\}$ NMR chemical shifts for **10-12** are summarized in Table 1, in the normal range of other four-coordinate Rh complexes of the type RhX_2L_2 .²⁶ For **12**, ${}^{31}\text{P}$ NMR shows a chemical shift of -26.0 ppm in CD_2Cl_2 , which is the highest field signal for all Rh-PTN(R) compounds reported.

Table 1: Solution ^{31}P NMR data for **2**, **10**, **11** and **12**. All signals are referenced with respect to 85% aqueous H_3PO_4 .

Compound	δ (ppm)	$^1J_{\text{RHP}}$ (Hz)	Solvent
2a	-91.8 ^a	-	C_6D_6
2b	-77.1 ^a	-	CDCl_3
10a	-48.2 ^b	151.2 ^b	C_6D_6
10b	-43.9 ^b	152.3 ^b	C_6D_6
11a	-40.2 ^b	143.5 ^b	CD_2Cl_2
11b	-37.4 ^b	142.3 ^b	CD_2Cl_2
12	-26.5 ^b	154.4 ^b	CD_2Cl_2

^a Reference 23. ^b This work.

^1H NMR chemical shifts are summarized in Table 2. ^1H - ^1H COSY and ^1H - ^{13}C HETCOR experiments were used to provide definitive assignments of the CH_2 groups of **2** in **11a** and **11b**. From the magnitudes of the $^nJ_{\text{PC}}$ it was possible to assign the CH_2 groups adjacent to phosphorus (Figure 1). For the resonances related to the CH and CH_2 groups of COD and **2**, there are significant differences between **11a** and **11b**, reflecting the rigidity of the PTN(R) framework, as it is apparent from Figure 2.

Table 2: Solution ^1H NMR data (δ , ppm, TMS referenced) for **2**, **10**, **11** and **12**.

Compound	$\text{CH}_2(\text{COD})$	$\text{CH}(\text{COD})$	$\text{CH}_3\text{-N}$	CH_2 (PTN(R))	$R\text{-P}$ ($^3J_{\text{PH}}$, Hz)
2a ^a	n/a	n/a	1.97 s	3.36-4.02	0.93d (5.40)
2b ^a	n/a	n/a	2.23 s	3.65-4.05	7.33-7.67
10a ^b	1.95-2.34	5.73 br s	2.22 s	3.02-4.26	1.14dd (6.60, 2.40 ^c)
11a ^a	2.25-2.57	5.26 br s	2.39 s	3.77-4.53	1.16d (9.90)
12 ^a	n/a	n/a	2.86 s	3.65-4.40	1.50 dd (10.46, 2.55 ^c)
10b ^b	1.89-2.32	5.77 br s	2.42 s	3.43-4.550	7.31-8.19
11b ^a	2.09-2.56	5.30 br s 3.56 br s	2.45 s	3.56-4.65	7.28-7.60

^a In CD_2Cl_2 solution. ^b In C_6D_6 solution. ^c $^4J_{\text{RH}}$

In **11b**, the CH_2 signals of COD (protons H_X and H_Y , Figure 1) show a complicated splitting pattern. Both the ^1H and ^{13}C NMR show that one set of the CH groups belonging to COD (H_Y ,

Figure 1) is shifted extremely upfield, $\delta(^1\text{H}_Y) = 3.559$ ppm (c.f. $\delta(^1\text{H}_X) = 5.303$ ppm) and $\delta(^{13}\text{C}) = 70.95$ (c.f. 109.12) ppm. These effects are attributed to ring current generated by the π -system of the phenyl substituent and its direct face-on positioning with respect to $(\text{CH})_Y$ group of COD, which is evident from the crystal structure of **11b** (*vide infra*). The chemical shift of the *P*-CH₂ groups of **2** (H_A and H_B) are less affected (and H_C to an even lesser extent) as observed by a different orientation from the phenyl group.

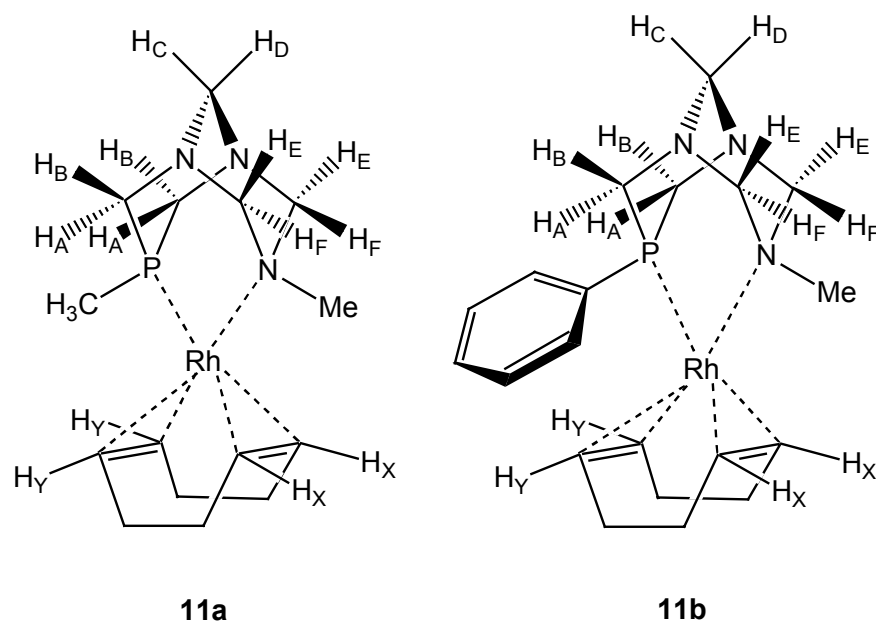


Figure 1: Labeling scheme of protons in the $[\text{Rh}(\text{COD})(\text{PTN}(\text{R}))]^+$ complexes **11a** and **11b**. The ring current effects of the phenyl group in **11b** significant alter the ^1H chemical shifts of H_A , H_B , H_C and H_Y .

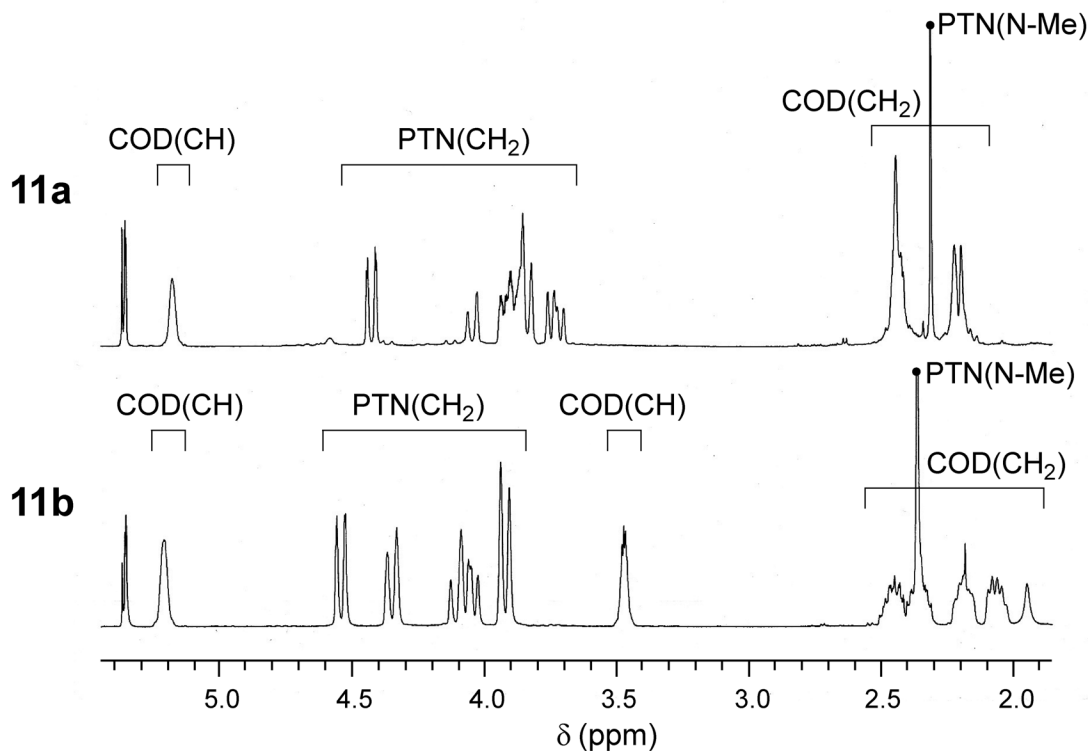


Figure 2: Comparison of the ^1H NMR spectra of **11a** and **11b** demonstrating the effects of the phenyl group in **11b**.

For **12**, the CO stretching frequency was observed at 1989 cm^{-1} in CH_2Cl_2 and at 1974 cm^{-1} in KBr, identical to that found in (*P*,*sp*²-*N*)-chelates of Rh(I) including $[\text{RhCl}(\text{CO})\{\text{P}(\text{Ph})_2\text{CPh}_2=\text{N}(p\text{-CNC}_6\text{F}_4)\}]$.²⁷

X-ray crystal structure determinations

Suitable crystals of **10**, **11** and **12** were grown and the corresponding X-ray crystal structure data were collected. Selected bond lengths and angles for all structures are provided in Table 3, while Table 8 (Experimental Section) summarizes the main crystallographic data.

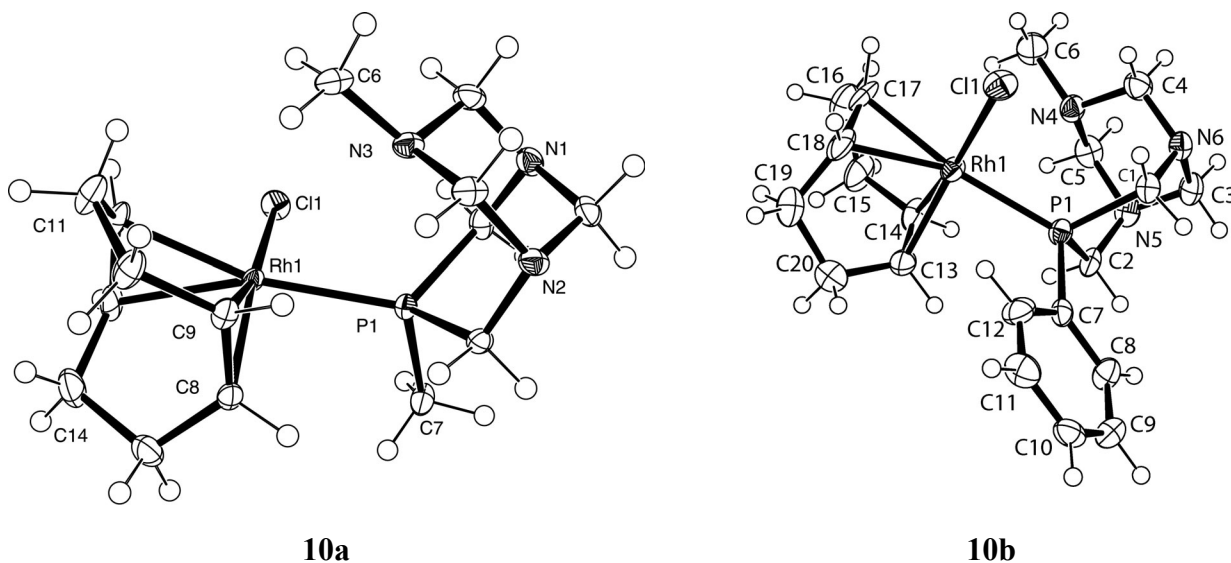
Table 3: Selected bond lengths (Å) and angles (°) for compounds **10**, **11** and **12**.

Parameter	10a	10b ^a	11a	11b	12
Rh-P	2.3073(5)	2.323(1)	2.334(1)	2.229(2) ^b	2.206(1)
Rh-Cl	2.3739(5)	2.394(1)	2.368(1)	-	-
Rh-I					2.711(5)
Rh-N	3.401(2)	3.055(2)	3.226(2)	2.204(3) ^b	2.213(3)
Rh-C	2.206(2)	2.189(4)	2.191(4)	2.229(5)	2.226(4)
(<i>trans</i> to P)	2.199(2)	2.179(4)	2.179(4)	2.230(5)	2.280(4)
Rh-C	2.108(2)	2.107(4)	2.116(4)	2.146(5)	2.155(3)
(<i>trans</i> to Cl or N)	2.107(2)	2.106(4)	2.098(4)	2.132(5)	2.130(3)
C=C	1.374(3)	1.385(6)	1.368(6)	1.353(8)	1.352(6)
(<i>trans</i> to P)					

C=C (<i>trans</i> to Cl or N)	1.409(3)	1.407(6)	1.407(6)	1.376(7)	1.406(6)	
Rh-C(O)						1.803(5)
Rh(C)-O						1.138(5)
P-Cexo	1.829(2)	1.829(4)	1.828(4)	1.775(5) ^b	1.813(4)	
P-Cendo	1.875(2)	1.870(4)	1.873(4)	1.800(5) ^b	1.844(4)	1.844(4)
	1.863(2)	1.864(4)	1.864(4)	1.805(5) ^b	1.853(4)	1.840(5)
N-Cexo	1.455(2)	1.465(4)	1.452(4)	1.525(6) ^b	1.498(5)	1.481(5)
N-Cendo	1.474(2)	1.475(4)	1.466(4)	1.570(6) ^b	1.512(5)	1.510(5)
	1.465(2)	1.472(4)	1.452(4)	1.577(6) ^b	1.517(5)	1.521(5)
Cl-Rh-P	87.58(2)	90.22(4)	89.07(4)	-	-	
I-Rh-N						98.7(1)
P-Rh-C(O)						90.6(2)
N-Rh-P	80.99(2)	62.65(4)	60.35(4)	83.3(1) ^b	84.1(1)	84.1(1)
Cl-Rh-N	95.05(2)	81.69(4)	60.33(4)	-	-	
C-Rh-C	81.7(2)	81.1(2)	81.9(2)	80.0(2)	80.5(1)	
	81.3(2)	81.8(2)	80.8(2)	79.9(2)	80.5(1)	
Cl-Rh-P-N	-97.6(2)	-80.5(1)	-81.7(1)	-	-	
Cl-Rh-C-P _{exo}	82.2(2)	93.1(1)	98.8(1)	-	-	

^a the two sets of parameters refer to the crystallographically independent molecules in the unit cell. ^b due to a statistical disorder between the terminal P and N atoms in this structure, the corresponding distances and angle are less reliable.

All compounds feature a square planar geometry, two coordination positions being defined wither by the centers of the C-C bonds of cod or, in the case of **12**, by iodide and CO ligands (Figure 3). Compounds **10** contain a coordinated P donor and a dangling N(Me) function, the fourth coordination position being occupied by the chloride ligand, whereas **2** adopts the κ^2 -*P,N* coordination mode in compounds **11** and **12** in keeping with the spectroscopic solution data.



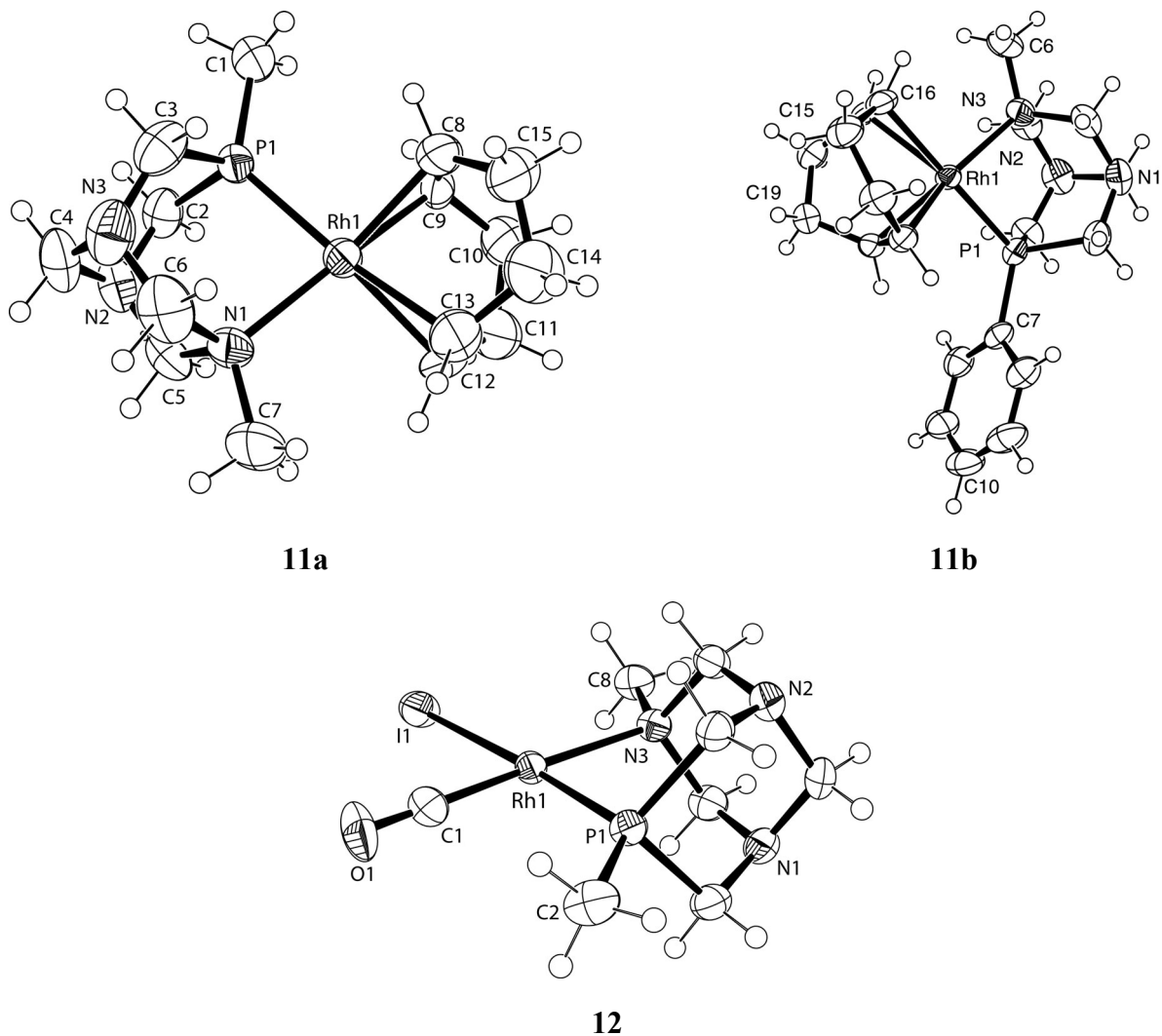


Figure 3: ORTEP diagrams of complexes $\text{RhCl}(\text{COD})(\text{PTN}(\text{R}))$ ($\text{R} = \text{Me}$, **10a**; Ph , **10b**), the cationic fragments, $[\text{Rh}(\text{COD})(\text{PTN}(\text{R}))]^+$ ($\text{R} = \text{Me}$, **11a**; Ph , **11b**) and the neutral complex $[\text{RhI}(\text{CO})(\text{PTN}(\text{Me}))]$ **12**. All diagrams are drawn with 50% probability ellipsoids. Hydrogen labels have been omitted for clarity. For **10b**, only one isomer is shown.

Complex **10a** shows intermolecular hydrogen bonding (3.045 \AA) between the rhodium center and the *N*-methyl group of $\text{PTN}(\text{Me})$ moiety, the hydrogen assuming an axial position with respect to the Rh center. The $\text{Rh}\cdots\text{N}$ distances (see Table 3) are approximately $0.4\text{-}0.8 \text{ \AA}$ shorter than the sum of van der Waals radii for Rh and N (3.800 \AA), suggesting the presence of a weak interactions between the Rh and N centers, due to the rigid ligand conformation and possibly shortened through crystal packing.

In **10b**, the majority of substituent orientations are identical among the two isomers present. The primary difference is in the rotation of the phenyl group, with Rh-P-C_{ipso}-C_{ortho} torsion angle at -12.09(5)° vs -29.40(5)°; in the former the phenyl group is almost coplanar with the bridgehead C, P and terminal N atoms, while for the second conformer it is almost eclipsed with the P-C bond of **2b**. An analysis of the crystal structure apparently showed no indications of disorder. The presence of the two different conformers is likely due to a small energy rotation barrier for the C(Ph)-P bond. The crystal packing forms a pseudo polymer (see Figure 4) where the units are sequentially linked through chloride-PTN interactions ranging from 2.734 to 2.910 Å. The different number of Cl[⋯]H (of the PTN fragment) interactions between units results in a variation in Rh-Cl bond length and phenyl group orientation within the individual conformers.

The Rh[⋯]N distances in **10a** and **10b** are significantly shorter than the distance between Rh and the dangling NEt₂ group in the [RhCl(CO){Ph₂PCH(*o*-C₆H₄NMe₂)CH(Ph)NPh}] complex (3.66 Å).¹⁸ The ligand is oriented such that it lies with the P,N vector orthogonal to the plane defined by the Rh, Cl and P centers. The Cl-Rh-P-N torsion angle is larger for **10a** (97.62(8)°) than for **10b** (86.52(15)°, 81.71(16)°). The Rh-P distance is slightly shorter for **10a**, 2.3073(5) Å, than for **10b**, 2.334(1), 2.323(1) Å. For **10a**, the shorter Rh-P bond results in a longer Rh[⋯]N interaction (3.401(2) Å) and a shorter Rh-Cl bondlength (2.374(1) Å). Both the longer P-Rh and shorter Cl-Rh bond lengths may suggest that **2b** is a slightly weaker electron donor than **2a**.

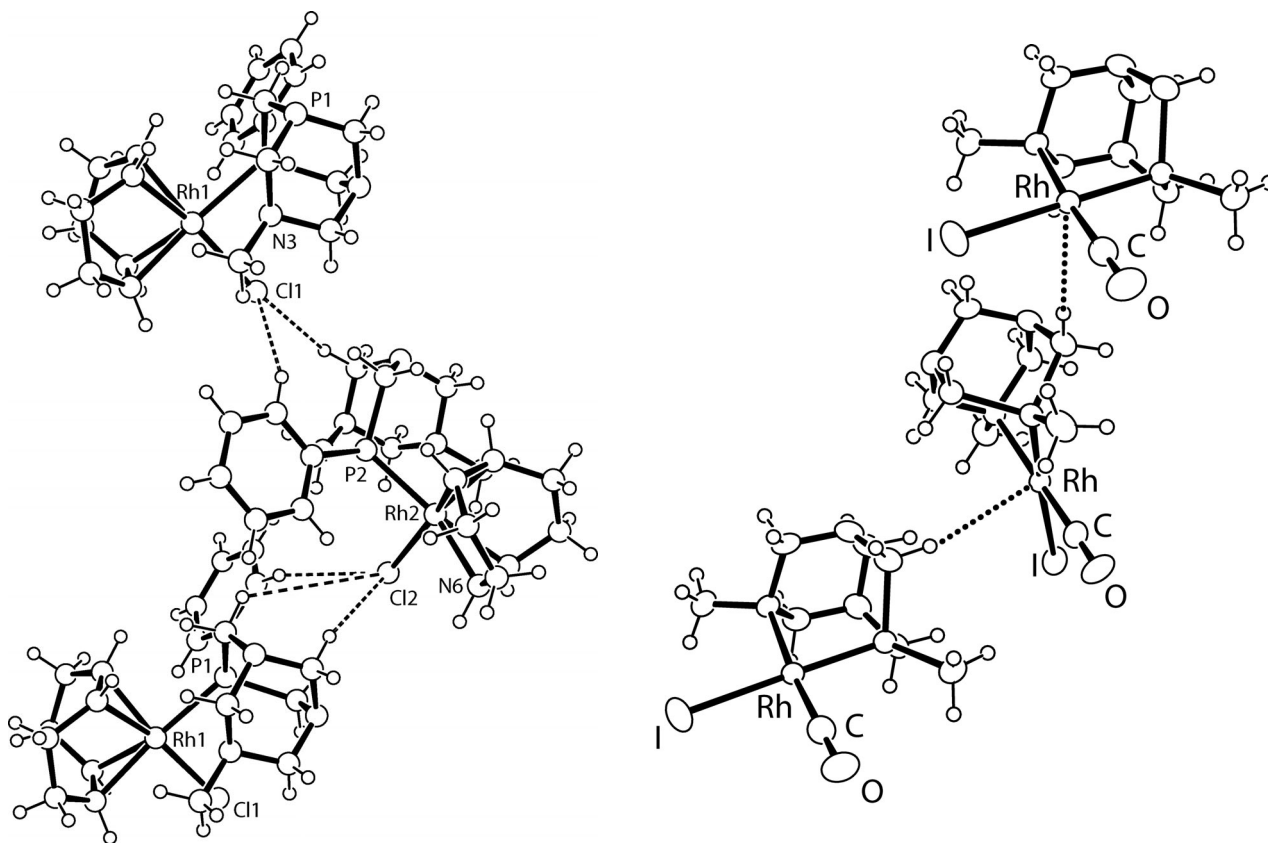


Figure 4: Left: Packing diagram (section) of **10b** highlighting the intermolecular interactions between hydrogen atoms of PTN(Ph) and chloride atoms. Right: Pack diagram (section) of **12** demonstrating the axial intermolecular interactions between the PTN(Me) and rhodium center.

A survey of the Cambridge structural database²⁸ shows to date 31 structures containing rhodium, COD, a non-bridging chloride and a mono-coordinating phosphine, the simplest being $[\text{RhCl}(\text{cod})(\text{PPh}_3)]$ ²⁹ having an identical Rh-P bond distance (2.308(2) Å) and a slightly longer Rh-Cl bond (2.361(2) Å) compared to **10a** and **10b**. However, comparison of the *P-trans* Rh-CH_(cod) distances shows that **10a** and **10b** have shorter distances than in $[\text{RhCl}(\text{cod})(\text{PPh}_3)]$ (2.205(7) and 2.238(7) Å) and corresponding a longer *P-trans* C(H)=C(H) bond (*cf.* $[\text{RhCl}(\text{cod})(\text{PPh}_3)]$ 1.340(10) Å).²⁹ The stronger π -back donation to COD indicates that the PTN(R) ligand is a stronger donor than PPh₃.

In **11** the cation and anion fragments are well separated from each other, the closest interactions being between H(PTN(R)) \cdots F(BAr^F₄) at 2.449 Å for both R = Me, Ph. The formation of the Rh-N bond is accompanied by a shorter Rh-P bond (see Table 3), *i.e.* approximately 0.1 Å shorter than that

of the parent compounds **10**. This result is consistent with the stronger ligand coordination characteristic of cationic rhodium(I) complexes.

The P-Rh-N bite angle for **11a** and **11b** (*ca.* 84°), is midway between the six (86.7°) and five membered systems (82.8°). A comparison of **10a** and **11a** with [Au{PTN(Me)}Me₂][AuMe₂Cl₂] reveals the P-M-N bond angles are identical²² within experimental error at a value of 82.7(5)°.

Due to the statistical disorder of the chelating P and N atoms within **11a** (described in the X-ray Structure Determination section), it is inconclusive whether the P-Rh and N-Rh distances are different from those of **11b**. The phenyl plane in **11b** is orthogonal to the plane defined by P, Rh and N and it is faced towards one side of COD. This observation is consistent with the NMR analysis showing downfield chemical shift and distributed resonances associated with COD and PTN(R) substituents (see above). This demonstrates that the phenyl group is maintained in an identical fixed position for the solution and in the solid state. Another interesting aspect of the structures of **11** is the significant increase in the P-C_{endo} and N-C_{endo} bonds (see Table 3) suggesting that **2** has been stretched in order to accommodate a chelating coordination mode. Analogous for compounds **10a** and **10b**, the Rh-C bonds are longer and the C=C bond is longer for the atoms of the COD ligand located *trans* to phosphorus.

In contrast to **11a**, **12** does not have disordering of P, N donor sites due the specific influences of the *trans*-effects caused by CO and I. Thus, the structure of **12** is significantly more reliable in terms of metric parameters associated with the chelated PTN ligand than **11a**. However, as a general observation, **11a** features shorter Rh-P and Rh-N bond lengths than **12**, which is consistent with stronger bonding associated with a cationic Rh center in the former. In comparison to RhCl(CO) complexes with **5**, **12** has both a longer Rh-P and Rh-N bond length, combined with a slightly wider P-Rh-N bond angle, moreover, the Rh-C(O) distance is shorter in **12** than in RhCl(CO) complexes with **5**. This suggests that **2** is a weaker ligand than **5**, and, probably, more hemi-labile. The internal PTN framework of **12** demonstrates some shortening in the P-C_{endo} and N-C_{endo} bonds, which is unresolved in the COD analog. The packing of the unit cell is similar to the other Rh-PTN complexes, containing weak intermolecular contacts between hydrogens of **2**. The most interesting property is an axial interaction between Rh and H3A (2.920 Å), which is continuously repeated as an

extended polymeric structure (Figure 4). A related example was reported in the *cis*-[PdCl₂(PTA)₂] structure where two strong Pd···H(CH) axial interactions (2.86 Å) form a dimeric unit.³⁰

Computational Analysis

A density functional theory investigation on **2a** and model complexes of **10a** and **11a** was performed in order to elucidate the electronic effects associated with *P*-coordination to Rh including the changes induced through κ^2 -*P,N* chelation. The complete **2a** ligand was optimized in *C_s* symmetry in the lowest energy configuration with *exo*-substituents on both P and N, which is the most suitable conformer for coordination. The energy-minimized model exactly matches the *exo,exo*-geometry observed in the disordered crystal structure reported by Schmidbaur and co-workers.²² Complexes of **10a** and **11a** were simplified by replacing COD by two ethylene groups, yielding the model complexes [RhCl(C₂H₄)₂{PTN(Me)}], **13**, and [Rh(C₂H₄)₂{PTN(Me)}]⁺, **14**. Complex **12** was modelled (**15**) without any simplifications, and is shown in Figure 5. In general, the optimized geometric parameters of **13**, **14** and **15** accurately represent the corresponding values experimentally observed for **10a**, **11a** and **12** within experimental error, especially those pertaining to the ethylene groups, **2a**, the P-Rh-Cl angle (for **13**), the P-Rh-N bite angle (for **14**) and the torsion angle of N-P-Rh-Cl. Minor over-estimations were observed for the Rh-P and Rh-Cl bonds (+0.02 and +0.01 Å respectively). A large variation, up to 7°, is noted with the C-Rh-C bond angles, probably caused by the replacement of the cyclic COD by two less constrained ethylene ligands.

The optimization of **14** in *C_s* symmetry, with the ethylene groups bisected by the N-Rh-P plane, yielded a saddle point with a corresponding single imaginary frequency of -60.2 cm⁻¹. Re-optimization in *C₁* resulted in a skewing of the ethylene groups within the square planar coordination geometry by 11.2°, as observed in the crystal structure of **11a**, yielding a stable minimum. Hence the distortion has an electronic origin related to rhodium coordination and does not result from the COD. The skewing energy is trivial and was calculated to be only 0.3 kcal mol⁻¹, which is in agreement with the fluxional behavior observed in solution. Indeed, the ¹H NMR spectra of **11** show only a single resonance for H_X and H_Y. Model **15** was optimized with *C_s* symmetry analogous to the crystal structure **12**, no imaginary frequencies were observed.

The HOMO of free **2a** consists of an out-of-phase combination of lone pairs associated with the three N atoms and a major contribution from the phosphorus lone pair (Figure 6). As in the case of the tightly constrained PTA, the intra-atomic repulsions between the two internal N centers and the terminal nitrogen and phosphorus centers are caused by the rigidly pinned structure of **2a**, thus resulting in a unusually higher energy expected for the HOMO.³¹ This is in line with the experimental observation that PTN is methylated at phosphorus rather than at nitrogen, as expected based on pure hard-soft rules.²² A single point calculation consisting of only the PTN(Me) fragment with the geometry fixed in the coordinating position observed in complexes **13** and **14** shows a 1.74 and 11.27 kcal mol⁻¹ difference in total energy from that of **2a**. Moreover, the energy of HOMO increased by 7.31 and 10.92 kcal mol⁻¹ respectively. A large portion of this energy change can be associated with an increase in bond strain when the internal framework of the ligand is stretched for metal coordination, especially high in the κ^2 -*P,N* chelating mode.

Mayer bond indices³² are particularly useful for measuring bond strain energy rather than bond lengths which in the case of the PTN(Me)-chelated complexes are unreliable due to site disorder between the coordinating P and N centers. Using the free **2a** as a reference point, continuing to P-coordination and finally to the P,N-chelate mode, the differences between **2a** and the **13**, **14** and **15** are presented in Table 4. It can be noticed that the P-coordination of PTN(Me) in **13** induces an overall bond strengthening within the ligand which can be attributed mainly to a substantial reduction in internal inter-atomic repulsion between P and N centers. In contrast, upon P,N-chelation in the cationic Rh complex **14**, a bond strength reduction occurs particularly for P-CH₂ and N_r-CH₂ and is counterbalanced by a strengthening of the N_r-CH₃ and P_r-CH₃ bonds. The bridgehead core component of the PTN ligand in all model complexes remains invariant to the mode of coordination and the oxidation state of the metal. Hence, when the PTN ligand is forced into a chelate mode to satisfy the electrophilic demand of the metal in **14** and **15**, both ends of the ligand are stretched to wrap around the Rh center. In comparison, the interaction between Rh and N_r is considerable weaker than that of the Rh-P. The increase for the latter from **13** to **14** does not affect the π -back-bonding to the *P*-trans ethylene ligand, as indicated by an almost identical C=C Mayer bond index for both species. Also expected is the increase of the Rh-P Mayer index on going from

14 to **15**, paralleling the bond shortening. The interaction between the N_t and Rh centers in **13** is extremely weak and practically non-existent as suggest by the Mayer bond index value.

An examination of the MO structure of **14** reveals a significant $\sigma^*(\text{P-CH}_2)$ contribution to the occupied SHOMO (second highest occupied MO), which is characterized by an interaction with the Rh d_{xy} orbital, see Figure 6. This type of occupation contributes significantly to the weakening of the P-CH₂ bonds as evidenced by the Mayer bond index. Certainly, the bond stretching associated to the chelation mode combines with the σ -electron withdrawing effect caused by the presence of the nitrogen atoms, to lower the energy of the $\sigma^*(\text{P-CH}_2)$ containing MO, which in turns promotes increased π -backdonation from Rh.

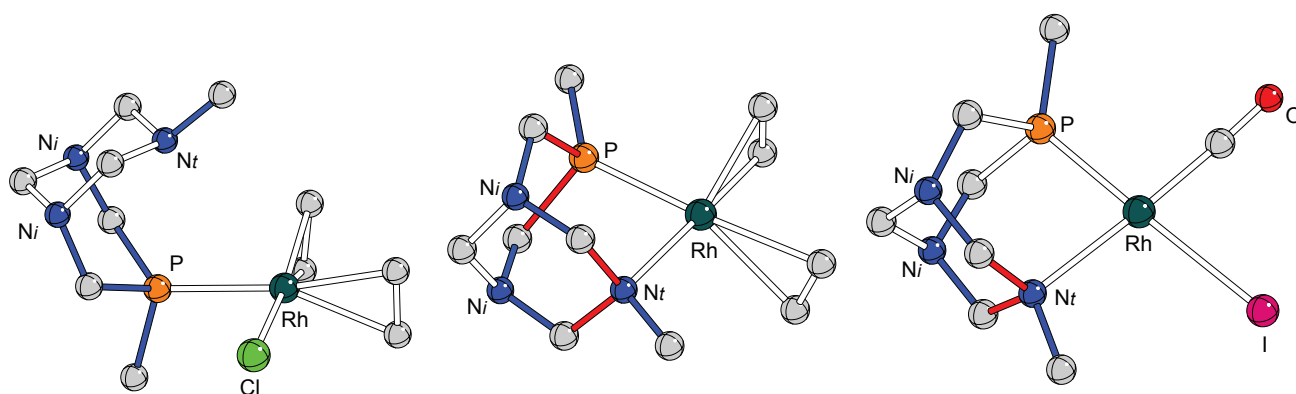


Figure 5: DFT Calculated geometries for **13**, **14** (representing simpler models of **10a** and **11b**) and **15** (unsimplified model of **12**). Unlabeled atoms refer to carbon. N_t and N_i denote terminal and internal nitrogen centers, respectively. Blue coloured bonds show those which are strengthened compared to the reference model, the uncoordinated PTN(Me) **2a**. Likewise, red bonds indicate those which have weakened compared to **2a**.

Table 4: Comparison of Mayer Bond Indices for the PTN(Me) ligand, free (**2a**) and ligated as through *P*-coordination **13**, and *P,N*-chelation **14**, **15**. For nitrogen labeling see Figure 5.

Parameter	2a	13	14	15
P-CH ₃	0.698	0.997	1.075	1.009
P-CH ₂	0.721	0.880	0.634	0.738
P-CH ₂ - N_i	0.828	0.868	0.693	0.881
		0.945	0.908	
		0.926	0.911	

$N_i-CH_2-N_i$	0.922	0.922	0.906	0.908
		0.924	0.915	
$N_i-CH_2-N_t$	0.872	0.909	0.981	0.971
		0.889	0.996	
N_t-CH_2	1.041	1.016	0.909	0.940
		1.024	0.908	
N_t-CH_3	0.801	0.879	0.940	0.939
Rh-P	n/a	0.825	1.201	1.379
Rh-N_t	n/a	0.015	0.222	0.234

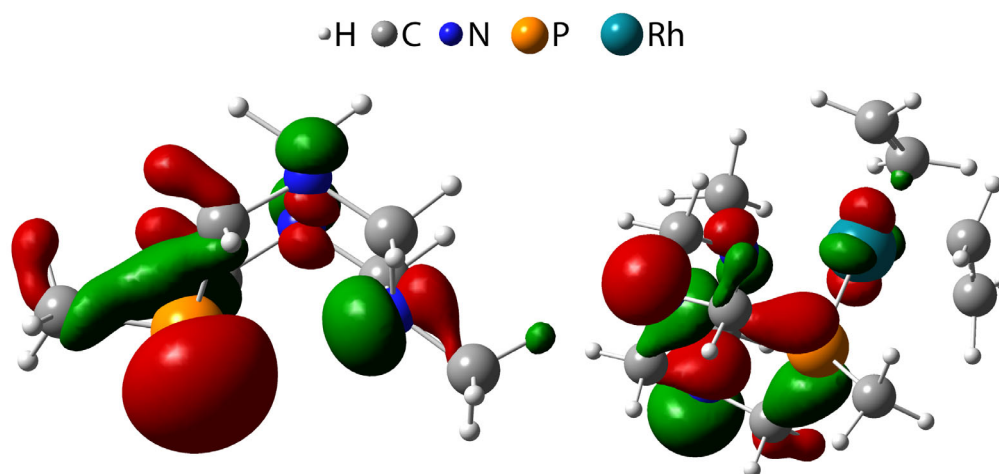


Figure 6: Left, The HOMO of PTN(Me) **2a** demonstrating the anti-bonding repulsions between the phosphorus and nitrogen atoms. Right, SHOMO of RhPTN(Me), **13** showing the orbital interaction between Rh d_{xy} and the $\sigma^*(P-C)$ of the PTN ligand which is partially responsible for weakening the P-C bonds. The other metal-ligand bonds have been omitted for clarity.

In summary, the DFT studies reveal significant changes to the PTN ligand on passing from the *P*-mono- to the *P,N*-chelating-coordination mode. Overall, it is evident that the PTN ligand has a preference for maintaining *P*-coordination to Rh. In contrast, a higher energy cost, in terms of bond strain, is associated with *P,N*-chelation which suggests that the ligand may show hemilabile behavior in the presence of polar solvents or other types of nucleophiles. Comparison of the Mayer bond indices for Rh-P and Rh-N bonds in cationic (**14**) and neutral (**15**) Rh(I) complex, indicates a stronger interaction with PTN in the latter complex, implying a higher tendency for hemilabile behavior for **14**.

Olefin hydroformylation tests

Complexes **10**, **11** and **12** were tested as catalysts for styrene and 1-hexene hydroformylation and transfer hydrogenation of benzylideneacetone (BZA) and acetophenone using $\text{HCO}_2\text{Na}/\text{H}_2\text{O}$ or $\text{KOH}/\text{Pr}^i\text{OH}$. The catalytic tests were carried out either using complexes formed *in situ* by addition of the ligands to either $[\text{RhCl}(\text{cod})]_2$ or $[\text{Rh}(\text{acac})(\text{cod})]$,³³ or by introducing the preformed complexes in the reaction mixture. It is well known that $[\text{RhCl}(\text{cod})]_2$ and Cl-containing phosphine adducts are a less suitable precatalysts than other Rh salts, because of the generation of strong acidity (HCl) under catalytic conditions.² However, the presence of external bases such as amines is often an efficient remedy and the use of hemilabile aminophosphine ligands has recently received considerable attention.^{18,34} The positive effect of the nitrogen donor basicity and proximity to the metal center has been demonstrated.^{34b} Therefore, a comparison of the activity for the Cl^- and acac^- precursors in the presence of ligands **2** was considered of interest.

Under mild hydroformylation conditions (CO/H_2 600 psi; CHCl_3 , 100 ml; 55 °C), using the complexes made *in situ*, the COD ligand will likely be replaced by CO. The runs were monitored by sampling the reaction mixtures and the conversion profiles are shown in Figure 7. The systems tested showed comparable efficiency (complete conversion after 8h), chemoselectivity (*ca.* 90% total aldehyde yield), and regioselectivity (b/l ratio *ca.* 91:9), without detectable traces of ethylbenzene among the (unidentified) by-products. No induction period was observed for the conversion of styrene. The conversion profiles are very similar, suggesting that the active species must be very close in nature for all the systems tested (Figure 7). Conversely, a blank test carried out with $[\text{RhCl}(\text{cod})]_2$ without **2** under identical experimental conditions showed that an induction period is required for aldehyde formation. These results are significant when compared with those recently reported in the presence of similar P,N ligands under essentially identical conditions, which showed no activity ($\text{TOF} < 1 \text{ h}^{-1}$) with PPh_3 from the chloride precursor.^{34b} That study has demonstrated that the TOF is sensitive to the distance between the N and P functions for amines of comparable basicity, proving that the proximity of the basic amine to the catalytic center has a beneficial role in the catalytic rate determining step. Only with ligand $\text{Ph}_2\text{PCH}_2\text{NMe}_2$ having the most basic amine in closest proximity to the phosphine donor was a similar activity observed for the chloride and acac catalytic precursors,^{34b} as observed in the present case for ligands **2**.

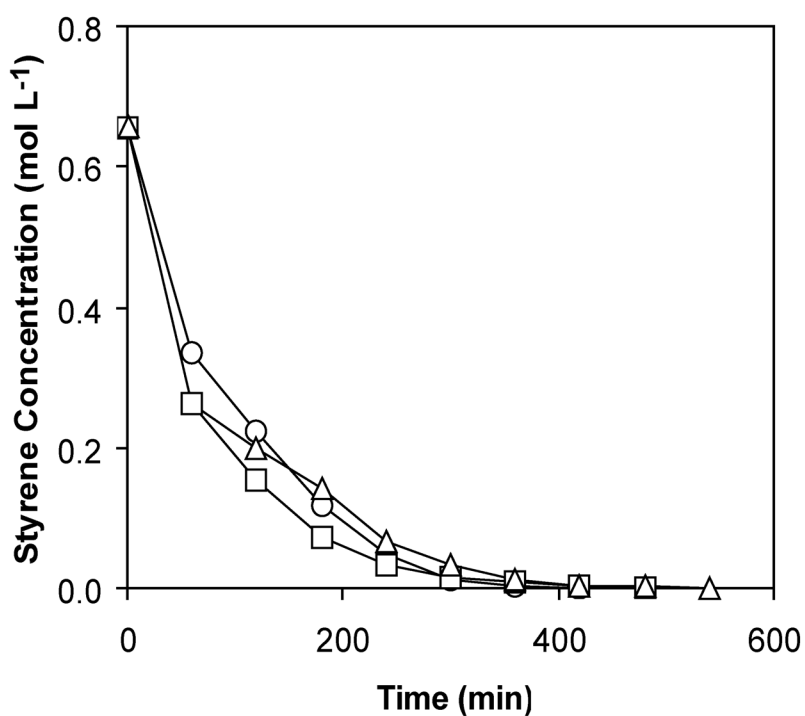


Figure 7: Reaction profiles for styrene hydroformylation in CHCl_3 at $55\text{ }^\circ\text{C}$. Run 1 (\square), $[\text{Rh}(\text{COD})\text{Cl}]_2 / \mathbf{2a} = 1:2$; run 2 (\circ), $[\text{Rh}(\text{acac})(\text{COD})] / \mathbf{2a} = 1:1$; run 3 (Δ), $[\text{Rh}(\text{acac})(\text{COD})] / \mathbf{2b} = 1:1$.

Styrene hydroformylation tests were then repeated in the presence of the preformed aminophosphine complexes and the final conversion and yields (no sampling) are reported in Table 5, both under strictly homogeneous (chloroform) and biphasic (*n*-octane/water) conditions. High conversions and chemoselectivity to the branched aldehydes (>94%) were achieved as expected for rhodium complexes and only traces of hydrogenated product (ethylbenzene, <0.5%) were determined. Control runs with $[\text{Rh}(\text{cod})\text{Cl}_2]_2$ showed that in CHCl_3 at $55\text{ }^\circ\text{C}$ a slightly higher l/b ratio is obtained at complete conversion (0.11, corresponding to 88.9% branched and 9.9% linear aldehyde), whereas in water/octane at $60\text{ }^\circ\text{C}$ a higher amount of ethylbenzene is produced (5.9% against 0.1 in CHCl_3) accompanied by a small increase in regioselectivity (l/b 0.08).

Preliminary mechanistic ^{31}P HPNMR studies in sapphire tube conditions showed that all phosphorus species are present in solution as doublets due to coupling with Rh during and after

exposing CHCl₃ solutions of the complexes to CO/H₂ pressure (600 psi) and prolonged heating to 55 °C, regardless from the presence of styrene.³⁵

Table 5: Styrene hydroformylation under homogeneous^a and biphasic conditions^b.

Complex	Conv. (%)	Branched (%)	Linear (%)	l/b	EtPh (%)
10a^a	99.3	95.4	3.7	0.039	0.2
10a^b	57.7	52.9	2.3	0.043	1.9
10b^a	88.4	84.5	3.7	0.044	0.2
10b^b	71.0	66.9	3.2	0.047	0.9
11a^a	80.8	74.7	5.5	0.074	0.5
11b^b	99.9	95.3	4.7	0.049	0.0
12^b	40.6	39.5	0.1	0.003	1.0

^a styrene: 2.5 mmol; cat: 0.01 mmol; H₂:CO (1:1), 600 psi; CH₃Cl: 40ml; 55 °C; 6 h.

^b as above, except H₂O/*n*-octane (2/1), 60 °C.

Further hydroformylation studies were carried out using 1-hexene as substrate, and the results are summarized in Table 6. As expected, the linear aldehyde is the favored product, with l/b ratio ranging from 1.35 (**10b** in CHCl₃, 4 h) to 3.13 (**10a** in THF, 1 h). The best conversion was achieved with **10b** (99%), although a larger amount of isomerized alkenes were found by GC analysis of the reaction mixture after the run. The composition of the syngas mixture has only a slight effect on the final conversion and yields, both being higher in the presence of CO/H₂ 1:1 mixture. The yield of isomerization is not largely affected by this variable. Remarkably, our systems afford very little amounts of hydrogenation products, except in the case when CHCl₃ is used as solvent at 55 °C instead of THF at 60 °C, where alcohols were also accounted for among the products.

Table 6: 1-hexene hydroformylation under homogeneous conditions^a.

Catalyst	Conv. % (h)	Linear %	Branched %	l/b	Isom %	Hydrog %
10a	20.2(1)	12.2	3.9	3.13	4.0	0.1
10a	61.5(4)	31.9	13.4	2.38	16.1	0.1
10a^b	83.0(4)	43.5	20.9	2.08	18.4	0.2
10a^c	92.5(4)	50.7	26.2	1.94	15.5	0.1
10b	63.4(1)	33.6	12.3	2.73	17.4	0.1
10b	99.3(4)	48.3	26.1	1.85	20.9	4.0
10b^c	82.5(4)	33.5	24.9	1.35	19.9	4.2 ^d
11a	27.4(1)	14.8	5.5	2.69	7.0	0.1
11a	70.0(4)	35.8	15.8	2.27	17.6	0.8
11b	52.6(1)	29.8	11.3	2.64	11.3	0.2

^a 1-hexene: 2.5 mmol; cat 0.01 mmol; H₂:CO (2:1), 600 psi; THF: 30 ml; 60 °C; 4 h.

^b CO/H₂ (1:1) 600 psi.

^c CHCl₃ 30 ml, 55 °C, CO/H₂ (1:1) 600 psi. ^d including alcohols.

The previously reported hydroformylation of 1-hexene with [Rh(acac)(CO)(PTA)] complex,³⁶ carried out in water, resulted in l/b ratio and TON in the same range as our set of catalysts. The catalytic styrene hydroformylation results are comparable with those reported by Andrieu *et al.*^{18,34b} using Ph₂PCH(*o*-C₆H₄CH₂NHPh) (**γ-P,N**) as ligand, for which HPNMR studies showed that under catalytic conditions it behaves as a monodentate phosphine, and this may imply a hemilabile nature of the PTN ligands in these reactions.

Transfer hydrogenation tests

The catalytic activity of Rh complexes in transfer hydrogenation reactions is well documented.³⁷ Complexes **10** and **11** were tested in the transfer hydrogenation of benzylideneacetone (BZA) and acetophenone. Very high chemoselectivity to C=C bond hydrogenation was obtained with all

complexes in the transfer reduction of BZA using NaHCO₂ as hydrogen source in water (Table 7). Interestingly, a ligand effect was observed on the conversion of BZA using **2a** instead of **2b**, regardless from the coordination mode of the ligand. The highest conversions (>95%) were observed in the presence of **2b**. Hydrogen transfer reduction of acetophenone was achieved using the KOH/PrⁱOH protocol (Table 7). Interestingly, good conversions (57-69%) were achieved using the monocoordinated Rh(I) neutral complexes **10** while moderate conversions were obtained with the cationic κ^2 -P,N chelated complexes **11**. At higher substrate/catalyst ratio (1000), hydrogen transfer to acetophenone still occurred albeit with lower conversion (20 %, TON 198). Cationic complexes **11** generally displayed TON values similar to the cationic aminophosphine rhodium precatalyst described by Gao *et al.*³⁸ Control experiments using [Rh(cod)Cl₂]₂ showed that BZA conversion was negligible under reaction conditions described in Table 7.

Table 7: Hydrogen transfer tests for the reduction of BZA^a and acetophenone^b.

Catalyst	Substrate	Conv. (%)	selectivity			Average TON
			% A ^c	% B ^c	% C ^c	
10a	BZA	59.9	98.6	1.4	-	60
10a	acetophenone	69.3	-	-	100	347
10b	BZA	96.4	99.8	0.2	-	97
10b	acetophenone	57.7	-	-	100	288
11a	BZA	59.3	98.8	1.2	-	60
11a	acetophenone	22.3	-	-	100	112
11b	BZA	100	>99.9	0.0	-	100
11b	acetophenone	17.4	-	-	100	87

^a BZA:catalyst:NaHCO₂ (100:1:1000); MeOH (3 ml); H₂O (3ml); 80 °C, 5 h.

^b Conditions: catalyst:acetophenone:KOH (1:500:5); PrⁱOH (10 ml); 80 °C, 6 h.

^c GC values based on pure samples. A = 4-phenyl-2-butanone; B = 4-phenyl-3-buten-2-ol; C = 1-phenylethanol.

CONCLUSIONS

In summary, a new class of Rh(I) neutral and cationic complexes bearing the water soluble aminophosphine cage ligand PTN have been synthesized, showing both $\kappa^1\text{-P}$ and $\kappa^2\text{-P,N}$ coordination modes. All the new PTN complexes were fully characterized by conventional spectroscopic methods in solution and by x-ray diffractometry in the solid state. The geometry of the ligand was correlated to the stability of chelation mode *vs* monocoordination by DFT calculations, suggesting that the straining constraints imposed by the rigid PTN ligand favors $\kappa^1\text{-P}$ coordination to Rh. The PTN ligand may behave as hemilabile under forcing olefin hydroformylation conditions and keep their $\kappa^1\text{-P}$ or $\kappa^2\text{-P,N}$ coordination mode during milder transfer hydrogenation of activated olefins and ketones. Mechanistic studies are currently in progress to verify this hypothesis.

ACKNOWLEDGEMENTS: We thank the EC for promoting this scientific activity with financial support including grants through the Marie Curie Research Training Network “Hydrochem” (contract HPRN-CT-2002-00176). Drs P. Barbaro, C. Mealli, (ICCOM-CNR) and Dr. E. Manoury (LCC) are gratefully acknowledged for extra NMR experiments and useful discussions regarding computational studies and catalysis. Dr C. Giannelli (University of Florence) is kindly acknowledged for supplementary GC analysis. Thanks are expressed to “FIRENZE HYDROLAB”, a project sponsored by Ente Cassa di Risparmio di Firenze, for supporting this research activity.

SUPPORTING INFORMATION Crystallographic information files (CIF) for **10a**, **10b**, **11a**, **11b** and **12**; coordinates for optimized models **2a**, **13**, **14** and **15**; full author list for Ref 47; experimental details for catalytic tests. This material is available free of charge via the Internet at <http://pubs.acs.org>.

EXPERIMENTAL SECTION

General Procedures

Manipulations of all products and reagents were carried under a purified N₂ or Ar atmosphere with standard Schlenk techniques. All glassware was pre-dried overnight and subsequently several purge/refill cycles were performed before the introduction of solvents or reagents. Toluene and *n*-pentane were dried by reflux over sodium, while dichloromethane was refluxed with CaH₂. All solvents were degassed prior to use. Styrene was purified by washing three times with 10% aqueous solution of NaOH followed by three washing with distilled water. After drying and filtration with MgSO₄, the styrene was twice trap to trap distilled under static vacuum and degassed for 30 minutes with a stream of argon. [RhCl(cod)]₂³⁹ and [Rh₂I₂(CO)₄]⁴⁰ were prepared in accordance with standard literature procedures. The aminophosphines **2a,b** were synthesized with a slightly modified procedure to that reported in the literature.^{17,22} NaBAR^F₄ was synthesized as described by Brookhart *et al.*²⁵ All other reagents (technical grade) were purchased from commercial sources and used as received. The NMR spectra were recorded using a Bruker AC-200 operating at 200 MHz, a VARIAN VXR instrument operating at 300 MHz or a Bruker Avance DRX operating at 400 MHz. Deuterated dichloromethane was dried with activated 4 Å molecular sieves and C₆D₆ with stirring over Na-K alloy. Both solvents were degassed prior to sample preparation. Chemical shifts for ¹H and ¹³C are referenced with respect to external TMS and ³¹P was referenced to external aqueous 85% H₃PO₄. FTIR spectra were measured on a Perkin Elmer Spectrum BX instrument using KBr pellets or solution cells. Elemental combustion microanalyses (C, H, N) were obtained using a Perkin-Elmer 2400 series II elemental analyzer. Mass spectra were obtained with a Nermag R10-10 mass spectrometer with the electron-impact technique. GC analyses were performed on a Shimadzu GC-14 A gas chromatograph equipped with a flame ionisation detector and a 30 m (0.25 mm i.d., 0.25 µm) film thickness) SPB-1 Supelco fused silica capillary column. GC/MS analyses were performed on a Shimadzu QP 5000 apparatus equipped with a column identical with that used for GC analysis.

Synthesis of [RhCl(cod){PTN(R)}] (10). In a dry and N₂ purged 50 mL Schlenk flask were introduced 0.493 g (1.00 mmol) of [RhCl(cod)]₂ and 5 mL of toluene. After 5 min of stirring, 2.00 mmol (**2a**, 0.346 g; **2b**, 0.471g) dissolved in 10 mL of toluene were added dropwise over a period of

30 minutes. After 1 h of stirring at room temperature, the volume of the solution was reduced to 5 mL under reduced pressure. Addition of 8 mL of *n*-pentane resulted in the formation of a yellow powder, which was collected by decanting off the mother liquor, washed with three 2 mL portions of *n*-pentane and dried overnight under vacuum.

R = *Me* (**10a**). Yield 0.748 g (93 %). Anal. Calcd. (found) for C₁₅H₂₈N₃PRh: C, 42.92 (43.02); H, 6.72 (6.32); N, 10.01 (9.70). Melting point (decomposition): 172 °C. ¹H NMR (299.96 MHz, 25 °C, C₆D₆) δ(ppm) = 1.14 (dd, 3H, ³J_{PH} = 6.6 Hz, ⁴J_{RhH} = 2.4 Hz, *P*-CH₃), 1.94 (m, 4H, CH₂(COD)), 2.22 (s, 3H, *N*-CH₃), 2.34 (br s, 4H, CH₂(COD)), 3.04 (m, 2H, *P*-CHH-*N*), 3.08 (m, 2H, *N*-CHH-*N*), 3.56 (m, 1H, *N*-CHH-*N*), 3.85 (m, 1H, *N*-CHH-*N*), 3.92 (m, 2H, *P*-CHH-*N*), 4.23 (m, 2H, *N*-CHH-*N*_{Me}), 5.72 (br s, 4H, CH₂(COD)). ¹³C NMR (75.43 MHz, 25 °C, C₆D₆) δ(ppm) = 28.95 (s, CH₂(COD)), 33.43 (s, CH₂(COD)), 38.86 (s, *N*-CH₃), 50.45 (d, ¹J_{PC} = 14.6 Hz, *P*-CH₃), 66.96 (d, ¹J_{PC} = 13.6 Hz, *P*-CH₂-*N*), 70.71 (d, ³J_{PC} = 10.8 Hz, *N*-CH₂-*N*), 76.47 (s, *N*-CH₂-*N*_{Me}), 98.98 (s, CH(COD)). ³¹P NMR (121.42 MHz, 25 °C, C₆D₆) δ(ppm) = -48.21 (d, ¹J_{RhP} = 151.2 Hz). MS (EI): *m/z* 419 (M⁺, 14.3%), 311 (M⁺-COD, 28.8%), 268 (M⁺-COD-CH₂NCH₃, 11.6%), 232 (M⁺-COD-CH₂NCH₃-HCl, 10.3%).

R = *Ph* (**10b**). Yield 0.863 g (89.6 %). Anal. Calcd. (found) for C₂₀H₃₀N₃PRh: C, 49.86 (49.82); H, 6.28 (6.12); N, 8.72 (8.31). Melting point (decomposition): 173 °C. ¹H NMR (299.96 MHz, 25 °C, C₆D₆) δ(ppm) = 1.90 (m, 4H, CH₂(COD)), 2.34 (br s, 4H, CH₂(COD)), 2.42 (s, 3H, *N*-CH₃), 3.44 (m, 2H, *P*-CHH-*N*), 3.92 (m, 1H, *N*-CHH-*N*), 4.13 (m, 2H, *P*-CHH-*N*), 4.53 (m, 2H, *N*-CHH-*N*_{Me}), 5.77 (br s, 4H, CH₂(COD)), 7.34 (m, 4H, *o,m*-C₆H₅), 8.16 (t, ³J_{HH} = 7.8 Hz, 1H, *p*-C₆H₅). ¹³C NMR (75.43 MHz, 25 °C, C₆D₆) δ(ppm) = 29.01 (s, CH₂(COD)), 33.17 (s, CH₂(COD)), 39.39 (s, *N*-CH₃), 49.32 (d, ¹J_{PC} = 10.71 Hz, *P*-CH₂-*N*), 68.05 (s, CH(COD)), 71.08 (d, ³J_{PC} = 9.60 Hz, *N*-CH₂-*N*), 76.10 (s, *N*-CH₂-*N*_{Me}), 97.77 (s, CH(COD)), 129.53 (s, *p*-C₆H₅), 131.42 (d, ¹J_{PC} = 85.01 Hz, *i*-C₆H₅), 132.75 (d, ³J_{PC} = 9.81 Hz, *m*-C₆H₅), 139.56 (d, ²J_{PC} = 15.61 Hz, *o*-C₆H₅). ³¹P NMR (121.42 MHz, 25 °C, C₆D₆) δ(ppm) = -43.90 (d, ¹J_{RhP} = 152.3 Hz). MS (EI): *m/z* 481 (M⁺, 0.85%), 373 (M⁺-COD, 10.1%), 330 (M⁺-COD-CH₂NCH₃, 9.8%), 294 (M⁺-COD-CH₂NCH₃-HCl, 12.2%).

Synthesis of [Rh(cod){PTN(R)}][BAR^F₄] (11). In a dry and N₂ purged 50 mL Schlenk flask were introduced 0.50 mmol of chloride precursor (0.210 g, **10a**; 0.241 g, **10b**) 0.432 g (0.50 mmol) of NaBAR^F₄, and 10 mL of dichloromethane. After overnight stirring at ambient temperature, the resulting cloudy solution was filtered to give a clear yellow solution. The volume of the solution was reduced to 4 mL under reduced pressure. The addition of 8 mL of *n*-pentane yielded a yellow powder, which was collected by decanting off the mother liquor, washed with three 2 mL portions of pentane, and dried overnight under vacuum.

R = *Me* (**11a**). Yield 0.487 g (78.2 %). Correct analytical data could not be obtained (low C, H, N), probably because of contamination by NaCl (the presence of sodium was confirmed by flame test). Melting point (decomposition): 97 °C. ¹H NMR (299.96 MHz, 25 °C, C₆D₆) δ(ppm) = 1.16 (d, 3H, ³J_{PH} = 9.9 Hz, *P*-CH₃), 2.292 (m, 4H, CH₂(C₈H₁₂)), 2.39 (s, 3H, *N*-CH₃), 2.534 (m, 4H, CH₂(COD)), 3.04 (m, 2H, *P*-CHH-N), 3.56 (m, 1H, *N*-CHH-N), 3.85 (m, 1H, *N*-CHH-N), 3.92 (m, 2H, *P*-CHH-N), 4.23 (br d, 2H, ³J_{HH} = 14.4 Hz, *N*-CHH-N_{Me}), 5.263 (br s, 4H, CH₂(COD)), 7.69 (s, 4H, *p*-C₆H₃(CF₃)₂), 7.85 (s, 8H, *o*-C₆H₃(CF₃)₂). ¹³C NMR (75.43 MHz, 25 °C, CD₂Cl₂) δ(ppm) = 29.59 (s, CH₂(COD)), 32.75 (s, CH₂(COD)), 46.97 (s, *N*-CH₃), 52.32 (d, ¹J_{PC} = 18.5 Hz, *P*-CH₃), 70.92 (s, *N*-CH₂-N), 74.28 (d, ¹J_{PC} = 11.7 Hz, *P*-CH₂-N), 80.79 (s, *N*-CH₂-N_{Me}), 109.29 (s, CH(COD)), 118.34 (s, *p*-C₆H₃(CF₃)₂), 125.49 (q, ¹J_{FC} = 272.5 Hz, CF₃), 129.75 (q, ²J_{FC} = 31.3 Hz, *m*-C₆H₃(CF₃)₂), 135.69 (s, *o*-C₆H₃(CF₃)₂), 162.64 (non binomial q, ¹J_{CB} = 49.8 Hz, *i*-C₆H₃(CF₃)₂). ³¹P NMR (121.42 MHz, 25 °C, CD₂Cl₂) δ(ppm) = -40.15 (d, ¹J_{RhP} = 143.5 Hz). The MS (EI) spectrum shows fragments deriving from the BAR^F₄ anion [m/z 796 (BAR^F₄-CF₃+2H, 2.3%), 777 (796-F, 1.5%), 727 (796-CF₃, 1.5%), 650 (BAR^F₃⁺, 5.4%), 631 (650-F, 7.5%)] but no fragments deriving from the cationic rhodium complex.

R = *Ph* (**11b**). Yield 0.475 g (72.6 %). Correct analytical data could not be obtained (low C, H, N), probably because of contamination by NaCl (the presence of sodium was confirmed by flame test). Melting point (decomposition): 128 °C. ¹H NMR (299.96 MHz, 25 °C, CD₂Cl₂) δ(ppm) = 2.12 (m, 2H, CH₂(COD)), 2.28 (m, 2H, CH₂(COD)), 2.45 (s, 3H, *N*-CH₃), 2.53 (m, 4H, CH₂(COD)), 3.56 (br s, 2H, CH(COD)), 4.01 (m, 2H, *P*-CHH-N), 3.92 (m, 1H, *N*-CHH-N), 4.14 (m, 2H, *P*-CHH-N), 4.53 (m, 2H, *N*-CHH-N_{Me}), 5.30 (br s, 2H, CH(C₈H₁₂)), 7.31 (t, ³J_{HH} = 7.8 Hz, 1H, *p*-C₆H₅), 7.57 (m, 4H,

o-,*m*-C₆H₅), 7.65 (s, 4H, *p*-C₆H₃(CF₃)₂), 7.85 (s, 8H, *o*-C₆H₃(CF₃)₂). ¹³C NMR (75.43 MHz, 25 °C, C₆D₆) δ(ppm) = 29.74 (s, CH₂(C₈H₁₂)), 32.40 (s, CH₂(COD)), 46.97 (s, *N*-CH₃), 51.29 (d, ¹J_{PC} = 16.6 Hz, P-CH₂-N), 70.95 (s, CH(COD)), 75.60 (d, ³J_{PC} = 11.8 Hz, N-CH₂-N), 80.80 (s, N-CH₂-N_{Me}), 109.12 (s, CH(C₈H₁₂)), 118.38 (s, *p*-C₆H₃(CF₃)₂), 132.71 (s, *p*-C₆H₅), 124.96 (d, ¹J_{PC} = 37.1 Hz, *i*-C₆H₅), 125.49 (q, ¹J_{FC} = 272.5 Hz, CF₃), 129.75 (q, ²J_{FC} = 32.2 Hz, *m*-C₆H₃(CF₃)₂), 130.46 (d, ³J_{PC} = 9.8 Hz, *o*-C₆H₅), 130.71 (d, ²J_{PC} = 7.8 Hz, *m*-C₆H₅), 135.69 (s, *o*-C₆H₃(CF₃)₂), 162.64 (non binomial q, ¹J_{CB} = 49.79 Hz, *i*-C₆H₃(CF₃)₂). ³¹P NMR (121.42 MHz, 25 °C, CD₂Cl₂) δ(ppm) = -37.36 (d, ¹J_{RhP} = 142.3 Hz). The MS (EI) spectrum shows fragments deriving from the BAR^F₄ anion [m/z 796 (BAR^F₄-CF₃+2H, 0.058%), 777 (796-F, 0.033%), 727 (796-CF₃, 0.037%), 650 (BAR^F₃⁺, 1.01%), 631 (650-F, 0.92%)], plus two fragments deriving from the cationic rhodium complex [1055 (M⁺-PTN(Ph)-F, 0.023%); 861 (1055-Ar^F-F, 0.048%)].

Synthesis of [Rh(CO){PTN(Me)}] (12). To a dry and N₂ purged 50 mL Schlenk flask, 57 mg (0.1 mmol) of [Rh₂I₂(CO)₄] was dissolved with 5 mL of dry and degassed toluene. To this solution, 36.7 g (0.21 mmol) of PTN(Me) in 5 mL of toluene was slowly added, and after 1 h stirring at ambient temperature, an orange precipitate was obtained. After removal of the mother liquor, the remaining solid was washed with three 2 mL portions of pentane and dried under reduced vacuum overnight. Yield 0.055 g (64%). Anal. Calcd. (found) for C₈H₁₆N₃OIPRh: C, 22.29 (22.45); H, 3.74 (3.89); N, 9.75 (9.70). ¹H NMR (400.13 MHz, 25 °C, CD₂Cl₂) δ(ppm) = 1.56 (dd, 3H, ²J_{PH} = 10.5 Hz, ³J_{RhH} = 2.6 Hz, P-CH₃), 2.86 (s, 3H, N-CH₃), 3.67 (br d, 2H, ²J_{HH} = 12.8 Hz, N-CHH-NMe), 3.74 (m, 1H, ²J_{HH} = 8.6 Hz, N-CHH-N), 3.78 (m, 1H, ²J_{HH} = 8.6 Hz, N-CHH-N), 4.04 (m, 2H_a+2H_b, P-CH_aH_b-N), 4.39 (d, 2H, ³J_{HH} = 13.0 Hz, N-CHH-NMe). ¹³C NMR (100.63 MHz, 25 °C, CD₂Cl₂) δ(ppm) = 29.68 (s, *N*-CH₃), (d, ¹J_{PC} = 22.5 Hz, P-CH₃), 56.25 (d, ¹J_{PC} = 30.2 Hz, P-CH₂-N), 70.79 (d, ³J_{PC} = 9.1 Hz, N-CH₂-N), 79.42 (s, N-CH₂-NMe) 189.91 (CO) ³¹P NMR (121.42 MHz, 25 °C, CD₂Cl₂) δ(ppm) = -25.98 (d, ¹J_{RhP} = 154.0 Hz). IR: ν_{CO} (cm⁻¹) = 1974 (KBr), 1989 (CH₂Cl₂).

X-ray Structure Determinations.

Large transparent yellow crystals suitable for single X-ray diffraction were obtained under air and moisture free conditions by slow diffusion of a layer of dry and degassed pentane into a saturated solution of dry and degassed solvents, toluene for **10a** and **10b** or dichloromethane for **11a**, **11b** and **12**. A single crystal of each compound was mounted under inert perfluoropolyether on the tip of glass fiber and cooled in the cryostream of an Oxford-Diffraction XCALIBUR CCD diffractometer for **10a**, **10b**, **11a** and **12** or a Stoe IPDS diffractometer for **11b**. Data were collected using the monochromatic MoK α radiation ($\lambda = 0.71073$). The structures were solved by direct methods (SIR97⁴¹ or SHELXS-97⁴²) and refined by least-squares procedures on F^2 using SHELXL-97.⁴² In **11a** and **11b** some CF₃ groups displayed very large anisotropic displacement parameters for the F atoms and they were then treated as disordered over two positions using the tools available in SHELXL-97. It is interesting to note that in compound **11a**, the isotropic thermal parameters for the P and N atoms coordinated to the rhodium displayed unrealistic differences thus indicating that the coordination sites are partially occupied either by P or N atoms. The P and N atoms were considered as sharing the same site and free refinement of the occupancy factors led to a P/N ratio of 90:10 on one site and 10:90 on the other site. All H atoms attached to carbon were introduced in idealized positions and treated as riding models. The drawing of the molecules was realized with the help of ORTEP3.⁴³ Crystal data and refinement parameters are shown in Table 8. Crystallographic data (excluding structure factors) have been deposited with the Cambridge Crystallographic Data Centre as supplementary publication no. CCDC *****. Copies of the data can be obtained free of charge on application to the Director, CCDC, 12 Union Road, Cambridge CB2 1EZ, UK (fax: (+44) 1223-336-033; e-mail: deposit@ccdc.cam.ac.uk).

Table 8: Selected crystallographic data for Rh(PTN(R))Cl(cod) (R = Me, **10a**; R = Ph, **10b**), Rh(cod)(PTN(R))[B(3,5-(CF₃)₂C₆H₃)₄] (R = Me, **11a**; R = Ph, **11b**) and RhI(PTN(Me))CO, **12**.

	10a	10b ^a	11a	11b	12
formula	C ₁₅ H ₂₈ ClN ₃ PRh	C ₄₀ H ₆₀ Cl ₂ N ₆ P ₂ Rh ₂	C ₄₈ H ₄₂ BF ₂₄ N ₃ PRh	C ₅₂ H ₄₂ BF ₂₄ N ₃ PRh	C ₈ H ₁₆ N ₃ OPRhI
fw, g mol ⁻¹	419.73	963.60	1332.44	1309.58	431.02
colour, habit	yellow, needle	yellow, prism	yellow, prism	yellow cube	orange prism
cryst syst	<i>P bca</i>	<i>P 2₁/c</i>	<i>P₋₁</i>	<i>P₋₁</i>	<i>Pbca</i>
space group	orthorhombic	monoclinic	triclinic	triclinic	orthorhombic
<i>a</i> , Å	15.3268(7)	9.9872(6)	13.3739(16)	12.2076(13)	12.5944(12)

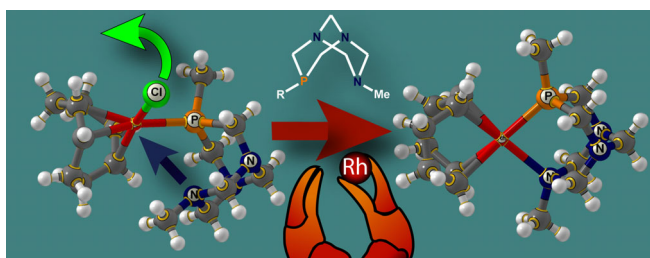
<i>b</i> , Å	18.0089(9)	12.8682(8)	14.1424(15)	14.7591(14)	12.1571(9)
<i>c</i> , Å	12.3321(6)	32.2080(19)	16.9699(19)	16.6244(18)	17.0443(14)
α , °	90	90	105.601(9)	73.349(12)	90
β , °	90	99.792(5)	98.540(10)	70.373(12)	90
γ , °	90	90	114.454(11)	88.792(12)	90
<i>V</i> , Å ³	3403.9(3)	4079.0(4)	2687.7(5)	2693.6(5)	2609.7(4)
<i>Z</i>	8	4	2	2	8
cryst dim, mm	0.14 × 0.0 × 0.02	0.23 × 0.21 × 0.06	0.4 × 0.26 × 0.11	0.2 × 0.16 × 0.12	0.2 × 0.16 × 0.12
<i>d</i> _{calc} , g cm ⁻¹	1.638	1.569	1.646	1.615	2.194
μ , mm ⁻¹	1.252	1.056	0.568	0.470	3.778
measured reflns	34414	28917	19023	26840	6852
unique reflns	5753	7997	9688	9859	2952
<i>R</i> ₁ [<i>I</i> > 2 σ (<i>I</i>)]	0.0272	0.0403	0.0500	0.0402	0.0344
<i>wR</i> ₂ , all	0.0579	0.0723	0.1120	0.1036	0.0840
S (GOF)	0.915	0.929	0.898	1.021	1.082
Parameters	192	471	861	851	138

^a two crystallographically independent molecules are present in the unit cell.

DFT Calculations

Geometry optimizations, Mayer bond indexes and energies were calculated with density functional theory using the Gaussian 03 suite of programs.⁴⁴ The three parameter hybrid gradient-corrected functional (B3P86) as developed by Becke⁴⁵ with the non-local correlation of Perdew⁴⁶ was used. For each step of the geometry optimizations, self-consistent iterations were performed until a convergence criterion of 10⁻⁸ was achieved. A double zeta gaussian-type basis set⁴⁷ was augmented with polarization functions⁴⁸ and with an additional set of d-orbitals for C, N and P and an additional p-orbital for hydrogen (6-31+G(d,p)). Rhodium was modeled with the LAN2DZ basis set of double zeta quality, substituting the core electron wave-functions with an effective potential.⁴⁹ Optimized structures were verified to be stationary minima as indicated by the absence of imaginary frequencies, except in the case of transition state (one imaginary was observed). Frequencies Simulated infrared spectra and reported frequencies values were corrected using a standard correction factor based on the level of theory and basis sets employed.

Graphical Abstract



The open cage PTN(R) ligands (PTN = 7-alkyl(aryl)phospha-3-methyl-1,3,5-triazabicyclo[3.3.1] nonane, R = Me, Ph) showed both $\kappa^1\text{-P}$ and $\kappa^2\text{-P,N}$ coordination to Rh(I). DFT calculations suggest a high strain of the $\kappa^2\text{-P,N}$ mode especially in the case of cationic complexes.

REFERENCES

- ¹ Slone, C. S.; Weinberger, D. A.; Mirkin, C. A. *Prog. Inorg. Chem.*, **1999**, *48*, 233 – 350.
- ² van Leeuwen, P. W. N. M.; Casey, C. P.; Whiteker, G. T. *Rhodium Catalysed Hydroformylation*; van Leeuwen, P. W. N. M., Claver, C., Eds.; Kluwer Academic Publishers: Dordrecht, The Netherlands, **2000**.
- ³ Agbossou, F.; Carpentier, J.-F.; Mortreux, A. *Chem. Rev.* **1995**, *95*, 2485.
- ⁴ Fache, F.; Schulz, E.; Tommasino, L. M.; Lemaire, M. *Chem. Rev.* **2000**, *100*, 2159.
- ⁵ For example: (a) Newkome, G.R. *Chem. Rev.* **1993**, *93*, 2067. (b) Anderson, M.P.; Casalnuovo, A.L.; Johnson, B.J.; Mattson, B.M.; Mueting, A.M.; Pignolet, L.H. *Inorg. Chem.* **1988**, *27*, 1649. (c) Jaaskelainen, S.; Haukka, M.; Riihimaki, H.; Pursiainen, J. T.; Pakkanen, T.A. *J. Organomet. Chem.* **2004**, *689*, 1064.
- ⁶ For example: (a) Ghilardi, C.A.; Midollini, S.; Moneti, S.; Orlandini, A.; Scapacci, G. *J. Chem. Soc., Dalton Trans.* **1992**, 3371. (b) Marxen, T.L.; Johnson, B. J.; Nilsson, P.V.; Pignolet, L.H. *Inorg. Chem.* **1984**, *23*, 4663.
- ⁷ Lee, H.-S.; Bae, J.-Y.; Ko, J.; Kang, Y. S.; Kim, H. S.; Kim, S.-J.; Chung, J.-H., Kang, S. O. *J. Organomet. Chem.* **2000**, *614*, 83.
- ⁸ (a) For example (a) Simonsen, K.P.; Suzuki, N.; Hamada, M.; Kojima, M.; Ohba, S.; Saito, Y.; Fujita, J. *Bull. Chem. Soc. Jpn.* **1989**, *62*, 3790. (b) Dahlenburg, L.; Gotz, R. *J. Organomet. Chem.* **2001**, *619*, 88. (c) Kashiwabara, K.; Morikawa, A.; Suzuki, T.; Isobe, K.; Tatsumi, K. *J. Chem. Soc., Dalton Trans.* **1997**, 1075. (d) Berger, H.; Nesper, R.; Pregosin, P.S.; Ruegger, H.; Worle, M. *Helv. Chim. Acta* **1993**, *76*, 1520.
- ⁹ (a) Kostas, I. D.; Screttas, C.G. *J. Organomet. Chem.* **1999**, *585*, 1. (b) McKay, I.D.; Payne, N.C. *Can. J. Chem.* **1986**, *64*, 1930.

-
- ¹⁰ Clarke, M.L.; Slawin, A.M.Z.; Wheatley, M.V.; Woollins, J.D. *J. Chem. Soc., Dalton Trans.* **2001**, 3421.
- ¹¹ (a) Butler, I.R.; Cullen, W.R.; Rettig, S.J. *Organometallics* **1986**, *5*, 1320. (b) Nishibayashi, Y.; Segawa, K.; Arikawa, Y.; Ohe, K.; Hidai, M.; Uemura, S. *J. Organomet. Chem.* **1997**, *545*, 381.
- ¹² For example, an interesting zwitterionic Indenide-Rh complex has been recently reported. Stradiotto M.; Cipot, J.; McDonald, R. *J. Am. Chem. Soc.* **2003**, *125*, 5619.
- ¹³ Phillips, A. D.; Gonsalvi, L.; Romerosa, A.; Vizza, F.; Peruzzini, M. *Coord. Chem. Rev.* **2004**, *248*, 955.
- ¹⁴ Smolenski, P.; Wajda-Hermanowicz, K. *J. Organomet. Chem.* **1998**, *570*, 1395.
- ¹⁵ Pruchnik, F. Smolenski, P.; Galdecka, E.; Galdecka, Z. *New J. Chem.* **1998**, *22*, 1395.
- ¹⁶ (a) Cermak, J.; Kvicalova, M.; Blechta, V. *Collect. Czech. Chem. Commun.* **1997**, *62*, 355. (b) Cermak, J.; Kvicalova, M.; Blechta, V. *Proceedings ISHC-10*, Princeton, NJ, **1996** (abstract B54).
- ¹⁷ Assmann, B.; Angermaier, K.; Schmidbaur, H. *J. Chem. Soc. Chem. Commun.*, **1994**, 941.
- ¹⁸ Andrieu, J.; Richard, P.; Camus, J.-M.; Poli, R.; *Inorg. Chem.* **2002**, *41*, 3876.
- ¹⁹ Faissner, R.; Huttner, G.; Kaifer, E.; Rutsch, P. *Eur. J. Inorg. Chem.* **2003**, 1681.
- ²⁰ Kuznetsov, V.F.; Facey, G.A.; Yap, G.P.A.; Alper, H. *Organometallics* **1999**, *18*, 4706.
- ²¹ (a) Bondoux, D.; Mentzen, B.F.; Tkatchenko, I. *Inorg. Chem.* **1981**, *20*, 839. (b) Pradat, C.; Riess, J.G.; Bondoux, D.; Mentzen, B.F.; Tkatchenko, I.; Houalla, D. *J. Am. Chem. Soc.* **1979**, *101*, 2234. (c) Wachter J.; Jeanneaux, F.; Le Borgne, G.; Reiss, J. G. *Organometallics* **1984**, *3*, 1034.
- ²² Assmann, B.; Angermaier, K.; Paul, M.; Riede, H.; Schmidaur, H. *Chem. Ber.* **1995**, *128*, 891.
- ²³ Fluck, E.; Weissgraber, H. *J. Chem. Ztg.* **1977**, *101*, 204.

-
- ²⁴ Darensbourg, D. J.; Joó, F.; Kannisto, M.; Katho, A.; Reibenspies, J. H.; Daigle, D. J. *Inorg. Chem.* **1994**, *33*, 200.
- ²⁵ Brookhart, M.; Grant, B.; Volpe, A. F. *Organometallics*, **1992**, *11*, 3920.
- ²⁶ Verkade, J. G.; Mosbo, J. A. Chapter 13 in *Phosphorus-31 NMR Spectroscopy in Stereochemical Analysis*, Verkade, J.G. and Quin, L. D. Eds, VCH: New York, **1987**.
- ²⁷ Katti, K. V.; Santarsiero, B. D.; Pinkerton, A. An.; Cavell, R. G. *Inorg. Chem.* **1993**, *32*, 5919-5925.
- ²⁸ (a) Cambridge Structural Database version 5.26 (February 2005). (b) Allen, F. H. *Acta Crystallogr.* **2002**, B58, 380. (c) Orpen, A. G. *Acta Crystallogr.* **2002**, B58, 398.
- ²⁹ Horn, Q. L.; Jones, D. S.; Evans, R. N.; Ogle, C. A.; Masterman, T. C. *Acta Cryst.* **2002**, E58, m51.
- ³⁰ Desiraju, G. R.; Steiner, T. *The Weak Hydrogen Bond*, New York: Oxford University Press, **1999**.
- ³¹ Phillips, A. D.; Peruzzini, M.; Mealli, C. EURESCO Conference, Sant Feliu de Guixols (Spain), 4-9 September 2004, Book of Abstracts, Poster 58 and unpublished results.
- ³² Mayer, I. *Int. J. Quantum Chem.* **1986**, *29*, 477.
- ³³ (a) Fornika, R.; Six, C.; Görls, H.; Kessler, M.; Krüger, C.; Leitner, W. *Can. J. Chem.* **2001**, *79*, 642. (b) Yamamoto, Y.; Fujita, M.; Miyaura, N. *Synlett* **2002**, 767. (c) Tanaka, M.; Hua, R. *Pure Appl. Chem.* **2002**, *74*, 181.
- ³⁴ (a) Camus, J. M.; Andrieu, J.; Richard, P.; Poli, R.; Baldoli, C.; Maiorana, S. *Inorg. Chem.* **2003**, *42*, 2384. (b) Andrieu, J.; Camus, J.-M.; Richard, P.; Poli, R.; Gonsalvi, L.; Vizza, F.; Peruzzini, M. *Eur. J. Inorg. Chem.* **2006**, 51. (c) Andrieu, J.; Camus, J. M.; Balan, C.; Poli, R. *Eur. J. Inorg. Chem.* **2006**, 62.

-
- ³⁵ Bosquain, S. S.; Phillips, A. D.; Gonsalvi, L.; Peruzzini, M. unpublished results.
- ³⁶ Pruchnik, F. P.; Smolenski, P.; Wajda-Hermanowicz, K. *J. Organomet. Chem.*, **1998**, 570, 63.
- ³⁷ (a) Toros, S.; Heil, B.; Kollar, L. *J Organomet Chem* **1980**, 197, 85. (b) Kollar, L.; Toros, S.; Heil, B. *J Organomet Chem* **1980**, 192, 253. (c) Spogliarich, R.; Kaspar, J.; Graziani, M. *J. Organomet. Chem.* **1986**, 306, 407. (d) Kvintovics, P.; Bakos, J.; Heil, B. *J. Mol. Catal.* **1985**, 32, 111. (e) Mestroni, G.; Zassinovich, G.; Alessio, E. *J. Mol. Catal.* **1989**, 49, 175. (f) Kvintovics, P.; James, B. R.; Heil, B. *J. Chem. Soc., Chem. Comm.* **1986**, 1810. (g) Leitner, W.; Brown, J. M.; Brunner H. *J. Am. Chem. Soc.* **1993**, 115, 152. (h) Thorpe, T.; Blacker, J.; Brown, S. M. *Tetrahedron Lett.* **2001**, 42, 4041. (i) Pamies O.; Backvall J. E. *Chem. Eur. J.* **2001**, 7, 5052. (i) Nindakova, L.O.; Shainyan, B.A.; Belonogova, L.N. *Russ. J. Org. Chem.* **2003**, 39, 1484.
- ³⁸ J.-X. Gao, X.-D. Yi, P.-P. Xu, C.-L. Tang, H.-L. Wan and T. Ikariya, *J. Organomet. Chem.*, **1999**, 592, 290.
- ³⁹ Giordano, G.; Crabtree, R. H. *Inorg. Synth.* **1979**, 19, 218.
- ⁴⁰ Fulford, A.; Hickey, C. E.; Maitlis, P. M. *J. Organomet. Chem.* **1990**, 398, 311.
- ⁴¹ Altomare, A.; Burla, M. C.; Camalli, M.; Cascarano, G. L.; Giacovazzo, C.; Guagliardi, A.; Moliterni, A. G. G.; Polidori, G.; Spagna, R. SIR97 a program for automatic solution of crystal structures by direct methods. *J. Appl. Crystallogr.* **1999**, 32, 115.
- ⁴² Sheldrick, G. M. SHELX97, Programs for Crystal Structure Analysis (Release 97-2); Institut für Anorganische Chemie der Universität: Tammanstrasse 4, D-3400 Göttingen, Germany, 1998.
- ⁴³ Farrugia, L. J. ORTEP3 for Windows. *J. Appl. Crystallogr.* **1997**, 30, 565.
- ⁴⁴ Gaussian 03, Revision C.02, Frisch, M. J. *et al*, Gaussian Inc., Wallingford CT, 2004.
- ⁴⁵ A. D. Becke, *J. Chem. Phys.* **1993**, 98, 5648.
- ⁴⁶ Perdew, J. P. *Phys. Rev B.* **1986**, 33, 8822.

⁴⁷ Francl, M. M.; Pietro, W. J.; Hehre, W. J.; Binkley, J. S.; DeFrees, D. J.; Pople, J. A.; Gordon, M. S. *J. Chem. Phys.* **1982**, *77*, 3654.

⁴⁸ Frisch, M. J.; Pople, J. A.; Binkley, J. S. *J. Chem. Phys.* **1984**, *80*, 3265.

⁴⁹ Hay, P. J.; Wadt, W. R. *J. Chem. Phys.* **1985**, *82*, 299.